BACTERIA MOBILITY IN THIN LIQUID FILMS AND NEAR A SOLID BOUNDARY

By

George B. Araujo

M.Sc., University of Sao Paulo, 2013

A dissertation submitted in partial fulfilment of the
requirements for the degree of Doctor of Philosophy
in the Department of Physics at Brown University

PROVIDENCE, RHODE ISLAND
May 2020

This dissertation by George B. Araujo is accepted in its present form
by the Department of Physics as satisfying the
dissertation requirement for the degree of Doctor of Philosophy

---

Prof. Jay X. Tang
Advisor
Date: _____

Recommended to the Graduate Council

Prof. Xinsheng Sean Ling
Reader
Date: _____

Prof. Thomas R. Powers
Reader
Date: _____

Approved by the Graduate Council

Andrew G. Campbell
Dean of the Graduate School
Date: _____

Thus if we enquire into the state of all dumb creatures, we shall find those fare best that are left to nature's conduct.

Erasmus

Aos meus pais

CV

Education

• Ph.D. (Physics), 2020, Brown University (defense in 2019)

• M.Sc. (Physics), 2013, University of Sao Paulo (USP)

• B.Sc. (Physics), 2011, Federal University of Rio Grande do Norte (UFRN)

Publications

- G. Araujo, W. Chen, S. Mani, J. X. Tang. Orbiting of flagellated bacteria within a thin fluid film around micrometer-sized particles. *Biophysical Journal*, 2019.

- G. Araujo, J. Zheng, J. X. Tang. Assessment of transient bacterial attachment to a solid surface by applying an electric field. *In preparation*.

- A. McMullen, G. Araujo, M. Winter, D. Stein. Osmotically driven and detected DNA translocations. *Scientific Reports*, 2019.

- J. Bell, G. Araujo, J. X. Tang. Rotational speed oscillations in body-tethered C. crescentus. *Under review*.

Teaching

• Physics II: Waves, Thermodynamics and Special Relativity (TA), USP, 2012.

• Calculus II and Calculus III (Main instructor), UFRN, 2014.

• Physics 0030: Basic Physics (TA), Brown University, Fall 2014, Spring 2019.

• Physics 0160: Introduction to Relativity, Waves and Quantum Physics (TA), Brown University, Spring 2015.

Presentations - during Ph.D

• Alignment and motion of uniflagellated bacteria in an electric field. American Physical Society March meeting. Los Angeles, CA, 2018.

• Orbiting of bacteria around micrometer-sized particles entrapping shallow tents of fluids. American Physical Society division of fluid dynamics meeting. Atlanta, GA, 2018.

• Detachment of uni-flagellated bacteria from a solid surface. American Physical Society March meeting. Boston, MA, 2019.

Ackowledgments

First of all, I would like to thank prof. Jay Tang for being a great advisor. I have learned a lot from our countless discussions on Science, being it about our own specific projects or in general. All these lessons will go with me as I move to other endeavors.

I am thankful to profs. Sean Ling and Thomas Powers for agreeing to be in my thesis committee. I also have gratitude to prof. Derek Stein, for the training in his lab and to prof. See-Cheng Ying for giving me advice in different moments during my stay at Brown University.

Regarding my lab training, I am in debt with Angus McMullen, for teaching me the initial steps. Laboratory work was more enjoyable thanks to the interactions with other labmates, among whom: Daniel Kim, Weijie Chen, Hui Ma, Jordan Bell, Chao Ji. I have also learned from the mentoring of undergraduate students: Michele Winter, Yingying Zhang and Joy Zheng, among others that I had a chance to collaborate in some way.

I highly appreciate the support from staff members in the Physics department that made the bureaucracy easier to deal with: Mary Ellen, Ida Alarcon, Barbara Cole. Not forgetting of Antonio Taylor who many times helped me to mail solid state chips around the country and even abroad.

I thank prof. Sridah Mani, from Albert Einstein College of Medicine in New York, for the collaboration in the Orbiting bacteria project, Geoff Wiliams from the Leduc Bioimaging Facility at Brown, for the acquisition of confocal images, Anthony McCormick for my initial training at the TEM and Matthew Huang from the University of Ottawa for the training in the Controlled dielectric breakdown project, not included in this thesis.

I thank all friends and colleagues I met during these years at Brown, among whom Tung Tran, Altan Allawala, Yehui He, Taka Kanaya, Kofi Acquah. Getting to know people from so many different cultures and backgrounds is one of the most valuable experiences I had in my phd.

I will always have fond memories of discussing the History of the Chinese empires, the particularities of the American culture or simply going on multicultural hikes in New Hampshire. I will hardly forget the ski trips to Wachussett, rowing at the Seekonk river, playing curling (!) at the Ocean state curling club or the several intramural soccer teams I took part at Brown. I will always remember the epic trip to see the Great American Eclipse in the middle of nowhere in 2017 and many other experiences during these years.

As the time to leave Providence gets closer, I'm left with bittersweet feelings. On one hand, I'm happy for finishing the degree, which was the main reason that brought me to this beloved town. On the other hand, deep down I know that some of the best years of my life are gone. The phd was not always easy, I did go through some ups and downs, but at the end of the day I thank my past self who years ago decided to apply to graduate school at Brown University, not really sure of what was going to happen, but confident that the potential experience would be worth a try.

TABLE OF CONTENTS

LIST OF TABLES

LIST OF FIGURES

CHAPTER 1
INTRODUCTION

This thesis consists of two main projects, presented in chapters 3 and 4, respectively. The first project describes bacterial confinement within a thin, but resilient, layer of liquid. The second project reports on the analysis of a transient state between attachment and detachment of bacteria from a solid surface while applying an external electric field.

Chapter 2 introduces experimental methods and physical concepts relevant to these projects. This chapter introduces two main types of bacteria cultivation used in this study: swimming microbes grown in dispersion medium and swarming colonies cultivated in semisolid agar gel. Theoretical concepts applied in chapters 3 and 4 are briefly described, namely, Darcy's law to describe fluid flow in porous medium, Young-Laplace equation to describe pressure difference across a concave liquid layer. Additionally, fundamental concepts in electrokinetics, particularly electrokinetic equations, are introduced.

In chapter 3, in the study of flagellated bacteria trapped within thin films of liquid, I describe observations on *Escherichia coli*, *Enterobacter sp*., *Pseudomonas aeruginosa*, and *Bacillus subtillis*, when they are confined within a thin layer of water around dispersed micrometer-sized particles sprinkled over a semi-solid agar gel. In this setting, *E. coli* and *Enterobacteria* orbit around the dispersed particles. The liquid layer is shaped like a shallow tent with its height at the center set by the seeding particle and the meniscus profile set by the strong surface tension of water. The tent-shaped confinement and the left handedness of the flagellar filaments result in exclusively clockwise circular trajectories. The thin fluid layer is resilient due to a balance between evaporation and reinforcement of fluid that permeated out of the agar. The latter is driven by the Laplace pressure caused by the concave meniscus. In short, I explain the physical mechanism of a convenient method to entrap bacteria within localized thin fluid film near a permeable surface.

In chapter 4, I investigate transient attachment of bacteria to a solid boundary. Bacterial attachment to surfaces is ubiquitous in nature and is the initial step to the formation of biofilms. Weak and reversible attachments constitute an early stage to permanent adhesion or a transient event on bacterial environmental exploration. Given that bacterial attachment has the potential to spoil surfaces or cause infection, different methods have been applied to find ways to remove bacteria from the surface they adhere to. Hence, I report an experiment for *Caulobacter crescentus* weakly attached to a plastic surface and subjected to an electric field parallel to the surface. I observe that some individuals transiently, but repeatedly attach to the surface. While electrophoretically driven by the field, these bacteria move significantly slower than the unattached ones and their speeds exhibit large variations, frequently dropping close to zero for short intervals of time. This study sheds light on the process of bacterial interaction with surfaces and suggests applying electric field as a useful method to investigate bacteria-surface interaction.

Chapter 5 states concluding remarks and offers perspectives based on the projects discussed in chapters 3 and 4. Some additional information is contained in the appendices, which include supplementary information for chapters 3 and 4 and also brief descriptions of side results that came out of the study of applying electric fields to bacterial cells. As a separate piece of theoretical work, one appendix provides a framework to numerically solve from scratch the Poisson-Boltzmann and the Conserved-Charge-Poisson-Boltzmann equations for a cylindrical channel.

CHAPTER 2

BACKGROUND

2.1 Bacteria dynamics and cultivation

This study deals with experiments of bacteria moving in shallow liquid tents and close to solid boundaries. In order to better explain the work, this section describes the essence of bacteria dynamics and the environmental conditions under which the microbes are grown.

2.1.1 Bacterial dynamics

From fluid physics perspective, the world for the tiny microorganisms we call bacteria looks rather different when compared to our own human experiences. In physical terms, it is said that these microbes live in the low Reynolds number regime. The meaning of this statement is that viscous forces dominate over inertial forces for bacteria, when considering water as their usual habitat. Reynolds number is a dimensionless quantity defined as $\mathfrak{R} = vR\rho/\eta$, dependant on the speed of the moving body *v*, a characteristic size scale *R*, the density ρ, and the viscosity of the medium η. For bacteria swimming in water, this quantity is on the order of 10^{-4}.

A consequence of living under these conditions is that in order to propel itself, a bacterium needs to continuously maintain its swimming activity. If the bacterium temporarily stops swimming, it would nearly immediately come to rest, in case diffusion could be ignored.

The swimming strategy at low Reynolds number has its peculiarities. It needs to be periodic, given the requirements to be continuous. The motion cannot be symmetrical, however, as that would lead to no net displacement. This was observed by E. M. Purcell in his groundbreaking paper ”Life at low Reynolds number” [1]. Contrary to the case of a

human being swimming, whose principle of motion is based on the time difference between movements of strokes and recoveries, an intrinsic inertial mechanism, a bacterium would ”lose” all its driving motion during the recovery step, i.e. it would advance during the strokes, but it would then return to its original position during the recovery.

Throughout their biological evolution, certain species of bacteria developed structures that enable them to perform non-symmetrical swimming patterns. Among these structures, a remarkable example, which is present in many species (including those used in this study) is the bacterial flagellum. Flagellum is typically a long filament (it can be several times longer than the size of cell body, which is under a few micrometers) attached to the cell surface. This filament is connected to a rotor, responsible for the driving motion. Some bacterial species, such as *Caulobacter crescentus* and *Pseudomonas aeruginosa*, have only one flagellum, which constrain their motility in the sense of limiting their ability to change swimming directions [2]. These species rely on the flexible hook at the base of their flagellum, allowing its bending to result in a flick [3], which changes the cell's direction of motion.

Other species, such as *Escherichia coli* or *Bacillus subtilis* have several flagella. E. coli in particular perform their well known [4] run and tumble motion cycles. Their flagella bundle together, spinning in the same direction during a run. They desynchronize during a tumble, which leads to a random change in their directions of motion.

Swimming propelled by flagellum comes from the thrust generated by the rotation of the filament. The reasons for swimming driven by motor propulsion have been widely discussed [5],[6],[4]. In summary, it is based on the fact that the drag experienced by a filament is larger when it moves sideways compared to when it moves parallel to the direction of the cell motion.

2.1.2 Bacterial culture

Bacteria are ubiquitous in all sort of environments on Earth. Some species adapted to live in extreme high temperatures, such as near underwater volcano vents [7] or in the extreme cold of Antarctica [8]. Their morphologies are adapted to their habitats. Given the relative short life cycles of bacteria (typically tens of minutes or a few hours [9]), it is possible to notice the differences in cell shapes when analyzing bacteria from the same original stock under different physical conditions. For instance, in this study, bacteria were grown under two sets of environments: in liquid suspension and on semisolid agar gels. When grown in liquid, bacteria have plenty of access to water and the diluted nutrients, whereas on agar gels, the water availability is limited and bacteria motion is severely constrained.

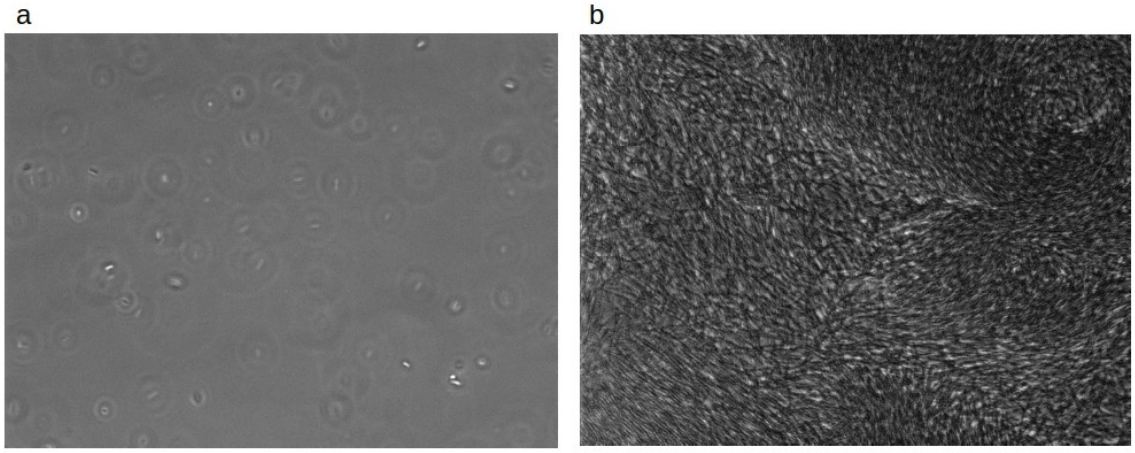

Figure 2.1: Pictures of *Enterobacteria* in (a) diluted suspension, represented by the white dots and in (b) dense swarming colony on agar gel

When in liquid medium, the predominant mode of bacterial motion is through swimming, as discussed in the previous section. This is the primary type of mobility at the level of individual cells. Cells also tend to be smaller in size when compared to cells grown in swarming colonies. Swarming colonies are, in our context, where cells collectively move on agar gels, facilitated by bacterial flagella. In this scenario the microorganisms predominantly move in packs called swarms as seen in Figure 2.1 (b). The expansion of the

bacterial colony comes from a combination of the group motion and the reproduction of the cells. When in swarms, the cells on the edge tend to be longer than those in the colony center, which may be attributed to suppression of cell division near the edge under these conditions [10].

On semisolid agar, bacteria need to extract water from the gel matrix. The flow of fluid in this setup has been thought [11] to be described in terms of Darcyś law. Bacteria secrete osmolytes which leads to an osmotic pressure that drives water from the bulk to the top of the gel, where the microbes predominantly populate.

2.2 Fluid flow in porous media and pressure gradient in a liquid meniscus

Some theoretical concepts are important for the understanding of the research described in the following chapters. Having that in mind, the next subsections will focus on reviewing ideas that will play key roles in the study of bacteria moving in shallow liquid tents. This introduction does not intend to be an extensive review, but a reminder of knowledge available in the scientific literature.

2.2.1 Darcy's law

The general approach to study fluid flow through a porous medium was empirically established by Henry Darcy in 1856 while investigating the hydraulic system in Dijon, France [12]. Darcy noticed a linear relationship between the flux through the medium (measured in units of volume/time) and the pressure drop along its extremities: $Q = \kappa A \Delta P / \eta L$. A is the cross section area of the pipe where the fluid flows, η is the fluid viscosity and L the characteristic length. Notice that Q/A has units of speed and can be understood as the fluid speed along its direction of flow. κ is a constant of proportionality known as the permeability of the medium. Darcy's law is applicable for laminar flow and is considered a coarse grained technique as it does not take into account details such as the channel structure and the fluid complexity [13]. One consequence of these limitations, for example, is

that Darcy's law fails to capture non-linearities such as in large deformations of porous media [14],[13]. This issue is overcome by applying more advanced concepts in the theory of elasticity to model the system of interest. For the purposes of this current study, Darcy's law is only used for estimating orders of magnitude of fluid and the porosity of an agar gel medium. Hence, we will stick to its classical definition. Figure 2.2 illustrates some parameters involved in the law definition.

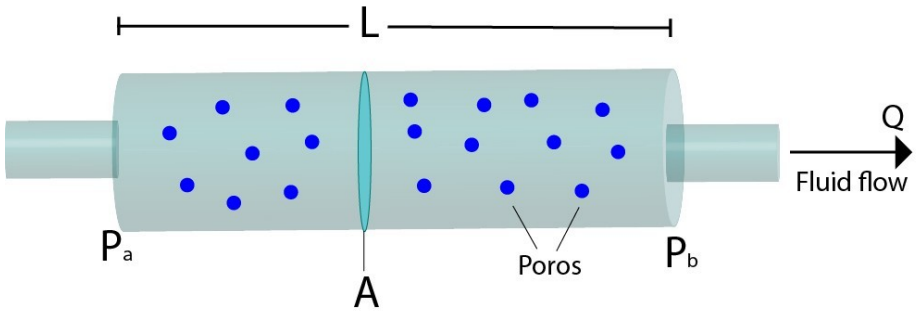

Figure 2.2: Representation of fluid flow through a porous medium with the pressure difference pumping the liquid through a pipe with cross-sectional area A and length L, as defined in Darcy's law, where Q is the flux.

2.2.2 Young-Laplace equation

Molecules in the liquid state attract each other through van der Waals forces or hydrogen bonds (for polar substances) forming a condensed structure strong enough to keep cohesion in spite of thermal agitation. This attraction happens in all directions for molecules in the bulk. However, when on the top surface of the liquid, molecules will only sense half of this effect, given that inter-molecular interactions will be restricted to other molecules on the surface and to those below the surface. This peculiar phenomenon gives rise to the surface tension of liquids. In water, for instance, the surface tension has the strength to allow some insects and spiders to walk on its top surface [15]. The surface tension can also be defined as the free energy per unit surface [16] and the shape that the liquid adopts at its surface leads to minimization of this free energy.

When there is a pressure difference in the interface of a liquid medium, the surface

curves in order to minimize its free energy (Figure 2.3). This situation is observed, for example, in the meniscus of liquid formed around a solid boundary. In 1804, Young and one year later independently, Laplace established the mathematical relation between the curvature of the liquid meniscus, its surface tension and the pressure difference. The relation, known as the Young-Laplace equation is defined as: $\Delta P/\eta = \kappa$, where again η represents surface tension and κ is the total curvature, which can be derived from the curvatures along the principal axes ($\kappa = 1/R_x + 1/R_y$).

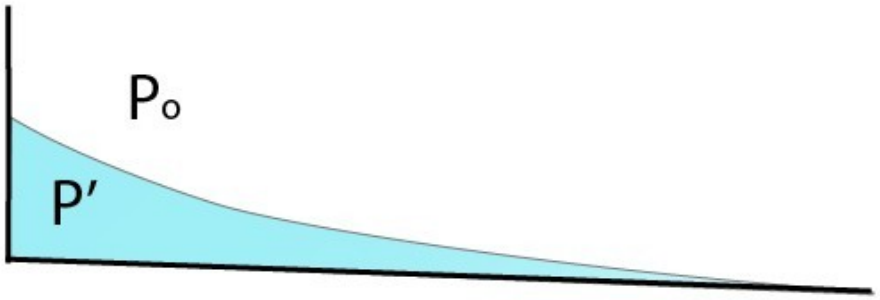

Figure 2.3: Illustration of the capillary effect. Water level rises near a solid wall. The internal pressure within the liquid film is lower than the external atmospheric pressure.

2.3 Electrokinetic concepts

Given the fact that bacteria have a surface charge when in aqueous environment, electric fields have been used for identification, separation and characterization of these microbes [17]. The study of the motion of charged particles driven by electric fields constitute what is known as eletrokinetics. Understanding the fundamental concepts of electrokinetics is an important step towards appreciating the ideas developed later in chapter 4, where we apply an electric field to assess bacterial interaction with surfaces.

2.3.1 Electrophoresis

Electrophoresis is the phenomenon of driven motion of colloidal or polyelectrolyte particles immersed in a liquid due to the application of an external electric field. At the low Reynolds

number regime with weak field intensities, there is a linear relationship between the particle speed and the strength of the electric field. The constant of proportionality in this relation is defined as electrophoretic mobility. In mathematical terms: $E = \mu v$, where *E* is the strength of the electric field, μ the electrophoretic mobility and *v* is the speed acquired by the driven particle. The electrophoretic mobility is a property of the moving particle, dependant on the medium where it is placed. Among different ways to apply a field to drive charged particles, here we focus on Capillary Electrophoresis, meaning that the electric field is applied along the long axis of a capillary channel.

2.3.2 Electroosmosis

Electroosmosis is the motion of liquid with respect to a reference at rest, such as the walls of the container holding the liquid, due to the an applied electric field. The explanation for this event comes from the fact that container walls are commonly charged when in contact with liquid (for example, silica SiO_2, which makes up the most common type of glass, exposes numerous SiO- ions on its surface). These charged surfaces attract counterions present in the liquid (such as H^+ in the case of water). Once the electric field is applied, these counterions will move accordingly (towards the negative pole for positive counterions or to the positive pole for negative counterions). The motion of the counterions will drag along liquid in their surroundings. Hence, electroosmosis plays a key role on defining the fluid flow pattern. For a constant field, electroosmosis establishes a flat flow profile, distinct from the parabolic profile seen in laminar flows driven only by a pressure difference among the capillary axis.

2.3.3 Electric double layer and Zeta potential

As briefly discussed in the previous subsection, the general framework to describe electrokinetic effects comes from the definition of a electric double-layer. The counterions that are attracted to a charged surface can be decomposed in two types: those in the immediate

vicinity of the surface are more strongly attracted and have limited mobility; they form the inner electric layer, also known as the Stern layer. In addition, there are counterions which are also attracted to the surface, but less strongly due to the shielding caused by the Stern layer. This second group form a diffusive, more mobile, layer that is largely responsible for the electroosmotic flow. The thickness of the electric double layer, a property of the particle charge and its medium, is known as the Debye length: $\lambda_D = \sqrt{\frac{k_B T}{2 N_A e^2 I}}$. In this expression, ϵ is the electric permitivity of the medium, k_B is the Boltzmann constant, *T* the absolute temperature in the unit of Kelvin, N_A is Avogadro number, *e* is the fundamental charge (of an electron, but omitting the negative sign) and *I* is the ionic strength of the electrolyte. The electrical potential difference between the surface of a charged particle and the end of the electric double layer is known as zeta potential. Notice that this idea of an electrical double layer applies to all charged surfaces in a medium containing an ionic solution. So, for charged colloids (or bacteria) in a glass container, there are electric double layers shielding both the surface of the container and the surface of the colloids. Figure 2.4 shows a schematic representation of an electric double layer.

2.4 Electrokinetic equations

The theoretical framework to deal with dynamic electrokinetic problems is to apply a system of coupled equations, namely: Nernst-Planck, Poisson and Navier-Stokes, with the fluid incompressibility condition. Wan et. al. [18] proposed the addition of a trap potential near the surface boundary to give rise to the charged layer of ions leading to electroosmotic effects. A framework to numerically solve the time independent electrostatic condition is described in Appendix D.

Nernst-Planck equation describes the charge dynamic of the system for charged species c_i, where **u** is the fluid velocity:

$$\frac{\partial c_i}{\partial t} + \mathbf{u}.(\nabla c_i) + \nabla . J_c = 0 \tag{2.1}$$

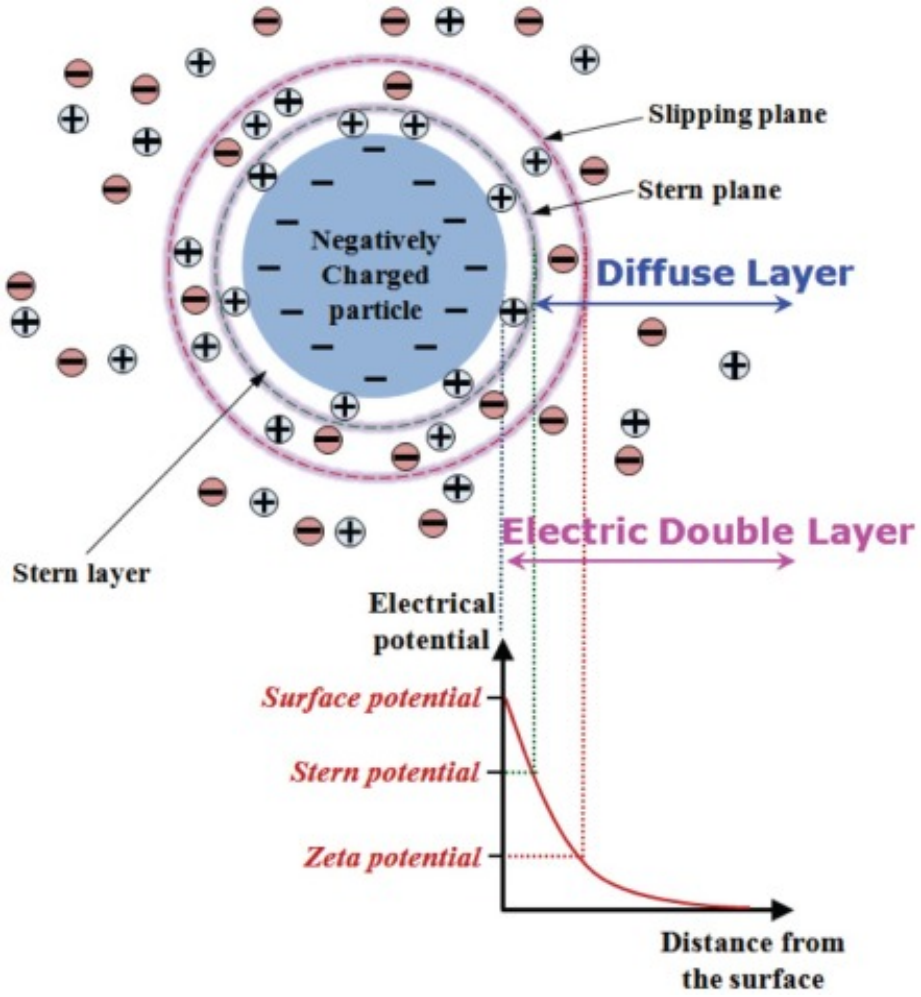

Figure 2.4: Schematic representation of an electrical double layer. Credit to: $https$: $//www.sciencedirect.com/topics/chemistry/electric-double-layer$

J_c is the current density for charged species c_i and it is defined as:

$$J_c = -D(\nabla c - \frac{e}{k_B T} c_i \nabla(\psi + f + g)) \tag{2.2}$$

In the equation above, D is the diffusion constant, e is the charge of one electron, k_B is the Boltzmann constant, T is the absolute temperature, ψ is the electrostatic potential originated from the ionic distribution, f is the surface trap potential and g is an external potential applied to the system, which in practice is provided by a power supply.

Wan et. al. [18] defined mathematically the trap potential for a cylindrical channel, in

cylindrical coordinates, with channel radius *a* as:

$$f(r) = \frac{\gamma}{2}(1 + cos(\frac{\pi(r-a)}{\Delta}), a - \Delta \leq r \leq a \tag{2.3}$$

$$f(r) = 0, 0 \leq r \leq a - \Delta \tag{2.4}$$

In the definition above, γ represents the "height" of the trap, i.e. the strength of ionic bonding to the surface and Δ is the trap "width", i.e. the distance from the surface where the trap potential is effective.

The electrostatic potential from the ionic distribution is expressed in terms of the Poisson equation, where *p* and *n* represent the charged distribution of the positive and negative ions and ϵ is the electric permitivity of the medium:

$$\nabla^2\psi = -\frac{e(p-n)}{\epsilon} \tag{2.5}$$

The fluid flow is governed by the Navier-Stokes equation, with the incompressibility conditions, where *P* is an external pressure, ρ is the fluid density and η is the fluid viscosity:

$$(\frac{\partial \mathbf{u}}{\partial t} + \mathbf{u}.\nabla\mathbf{u}) = -\nabla P + \nabla^2\mathbf{u} - e(p-n)\nabla(\psi + f + g) \tag{2.6}$$

The incompressibility condition is given by:

$$\nabla.\mathbf{u} = 0 \tag{2.7}$$

When there is no time dependence for the ionic distribution, meaning that the fluid is at rest, the model from a classical perspective simplifies to that of the Poisson-Boltzmann equation (PB). A modified version of this equation that takes into account charge conservation within the computational domain, the Conserved Charge Poisson-Boltzmann (CCPB) is solved numerically in appendix D, including the trap potential.

CHAPTER 3
ORBITING OF FLAGELLATED BACTERIA WITHIN A THIN FLUID FILM AROUND MICROMETER-SIZED PARTICLES

3.1 Introduction

Hydrodynamics and confinement dominate bacterial mobility near solid or air-water boundaries, causing flagellated bacteria to move in circular trajectories. A flagellated bacterium propels itself by rotating its flagella relative to its body, which counter-rotates [5]. Freely swimming bacterial cells tend to accumulate close to solid surfaces [19, 20, 21], with their residence times within a few micrometers (up to 1-3 μm) from the boundary lasting several seconds [22]. The coupling of body rotation and the enhancement in the drag force exerted on the part of the cell closer to the solid surface causes the bacterium to move in circular trajectories [23, 24]. The handedness of the flagella determines whether the circular trajectory is clockwise or counterclockwise. *E. coli*, for example, moves forward in clockwise paths when looked from above [25], propelled by its flagellar filaments with left-handed helical structure; for the same reason, it swims on the right-hand side when prevented to turn by a solid wall on its side [26].

Numerous experimental techniques, including microfluidic devices [27, 28], droplets [29, 30, 31, 32], or vortices [33], have been developed to confine and maneuver motile bacteria. The mode of bacterial motility can also be shaped by confinement. For example, whereas flagellated bacteria swim in liquid, they may move collectively on a solid surface in the form of swarming motility [34, 35, 36, 11]. The swarming motility triggers a variety of adhesive mechanisms, including those preceding to the growth of biofilms [37, 38, 39]. Therefore, the study of bacterial near surface motility has broad implications such as in biofouling [40] and infection [41].

This report describes swimming motility of flagellated bacteria in shallow tents of liquid films seeded by graphite particles or glass beads a few microns in diameter. Around these particles sprinkled over the agar surface, one or more bacteria move in persistent circular trajectories for over several minutes. We account for the observed phenomenon with a physics-based model, encompassing hydrodynamic analysis, surface tension, evaporation, and porous flow. We also discuss broad implications of the mechanism elucidated by this study.

3.2 Materials and Methods

3.2.1 Bacterial strains

Six strains of bacteria were used. Strain HCB33 (wild type *E. coli*) was acquired from Howard Berg (Harvard University). *P. Aeruginosa* PAO1 was provided by Keiko Tarquinio (Emory University Medical School). *B. subtillis* 3610 was obtained from Daniel B. Kearns (Indiana University). The remaining three strains were isolated at the Albert Einstein College of Medicine (NYC). Specifically, H5 is a swarming strain of *E. coli* from human feces (Committee on Clinical Investigation CCI# 2009-446-006; IRB# 2015-4465); SM1 and SM3 are novel strains of swarming *Enterobacter sp.* isolated from mouse feces (presently undergoing species characterization).

3.2.2 Sample preparation

Bacteria (with the exception of *P. aeruginosa*) were grown in suspensions of Lysogeny Broth (LB) medium overnight ($\approx$ 16 hours) and then a $5\,\mu\mathrm{L}$ droplet was taken to inoculate the center of a petri dish containing LB agar gel (LB + 0.5% agar). Triton-X100 (Sigma-Aldrich) was added (0.1% in volume) to the LB agar as external surfactant for *E. coli* inoculation in order to accelerate its colony spread. In particular, it was observed for the H5 strain that with the addition of triton, the colony spreads in similar rate to what is seen in typical species of swarming bacteria: it populates the whole petri dish ($\approx$ 10 cm in

diameter) within a few hours. For the HCB33, the effect of triton addition was not as dramatic and the colony grew only slightly faster compared to when no external surfactant is added to the growth medium. *P. aeruginosa* was grown overnight in suspension of Tryptic Soy Broth (TSB) and then a $5\,\mu\mathrm{L}$ droplet from the culture was inoculated on a petri dish containing TSB agar gel (TSB + 0.5% agar).

The samples were placed into an incubator with controlled temperature of 37^{o}C and 50% relative humidity for 3 to 5 hours, depending on the growth rate. In the next step, a droplet containing micrometer-sized particles (graphite or silica beads) was placed at a location close to the swarm front so that the region where the droplet spread overlapped with the colony, as illustrated in Figure 3.1 a. Graphite particles were obtained by scrapping a pencil with a razor blade and dispersed in deionized water (DI water). Silica beads ($4.5\,\mu\mathrm{m}$ in diameter, Bangs Laboratories, Inc) were also diluted in DI water. After the addition of the water droplet, the petri dish was gently tilted in different directions to guide the droplet to spread away from the bacterial colony. This motion created thin water layers that evaporated within a minute or two on the agar surface. Most bacteria then got stuck on the dried surface, leaving a small number of swimming bacteria trapped in shallow films of water around the dispersed particles.

3.2.3 Imaging, measurements and graphic illustrations

Particles and bacteria on the agar surface were imaged under an upright microscope (Nikon Eclipse E800) with a 40x objective lens, coupled to a CCD camera (Photometrics Coolsnap EZ). The imaging was controlled by the software Metamorph (Molecular Devices) through which the movies were recorded. The recording rate was in the range between 10.72 frames per second (fps) and 33.88 fps, with lower frame rates chosen for larger imaging areas, as needed.

Radius of meniscus was determined by identifying five nearest immobilized bacteria around a particle and averaging their distances from the center of the particle. In rare

cases the average was obtained from only 3 or 4 distances, as the number of immobilized bacteria in the surroundings was lower than five. Thus, our estimate was limited by the optical microscopy images acquired. A full meniscus profile, as the one obtained with x-ray microscopy in [42] could expand beyond the region defined in this study. Bacterial trajectories and their swimming speeds were calculated using ImageJ from their captured positions in video clips. The numerical calculation applying Resistive Force Theory was implemented in a Python code.

Confocal microscopy was done using an Olympus FV3000 laser scanning microscope with excitation wavelengths of 488 nm and 561 nm. The procedure follows a previous publication [43], but modified due to the peculiarities of our system. In order to label the agar gel, 0.1 mg/mL solution of Nile Red in methanol was mixed in a proportion of 1:100 volume/volume into LB agar in hot liquid state. Then, 20 µL of the mixture was deposited on a FluoroDish (World Precision Instruments), forming a very thin layer of gel (on the order of 100 µm). Such a thin gel was required for confocal imaging using the inverted microscope, so that the gel surface was within the focal depth of a 60x objective lens. In this setting, the transmission lights travel through the gel to enter the objective without being refracted by the large beads sitting on the gel surface. Due to evaporation of fluid in the thin gel, however, there is a limited time window for sample preparation and confocal imaging. Right after the gel was pulled, a mixture of 4.5 µm silica beads and 0.5 µm fluorescent Dragon Green beads (Bangs Laboratories Inc.) at a ratio of 1:2000 was added on top of the gel. The smaller beads serve as an additional label for tracing the gel surface. The Dragon green dye was excited by both blue and green lights, but more strongly by blue to emit green light. Nile red was mainly excited by green light, emitting red light. Image analysis and processing were done using ImageJ. Adobe Illustrator was used to vectorize images of orthogonal slices of the data and obtain middle lines through a high intensity band on these images, locating the gel surface.

In order to convey physical pictures of bacteria and liquid films, which are invisible

under optical microscopy, several figures include illustrations generated using Rhinoceros, a CAD software widely used by architects and designers. Indications are made in respective figure captions where secondary features may have been omitted in those illustrations for the sake of simplicity.

3.2.4 Hydrodynamic model

E. Lauga *et al.* proposed a model based on Resistive Force Theory to represent bacteria moving close to solid boundaries [44]. It models a bacterium as formed by a sphere connected to a helical rod, to represent the cell body and flagella bundle, respectively. The free swimming organism is subjected to zero net force and torque, and is propelled by the rotating flagellar bundle. Body and flagella are characterized by their respective mobility matrices, which appear in the linear system of equations, equation 3.1, given the velocities and rotation rates of the cell body in equations 3.2 and 3.3, respectively.

$$(A + B)X = BY \tag{3.1}$$

where,

$$X = (Ux, Uy, Uz, \Omega x, \Omega y, \Omega z)^T \tag{3.2}$$

$$Y = (0, 0, 0, 0, \omega, 0)^T \tag{3.3}$$

Matrix *A* is the mobility matrix of the cell body. *B* is the mobility matrix of the flagella. U_i gives the i-th component of the velocity and Ω_i the i-th component of the rotation rate of the cell body. The rotation rate of the flagella is given by ω. The cell is set to initially align with the y axis, without loss of generality. Reference [44] gives the details on how to build the mobility matrices.

The velocities and rotation rates in this model are dependent on the gap distances

between the surface and the material parts of the model bacterium. The speed U of the bacterium in circular motion is given by the components along the bottom surface: $U = (Ux^2 + Uy^2)^{1/2}$ and the radius of curvature R of the cell trajectory is also obtained from the solution of the linear system: $R = U/|\Omega_z|$.

3.3 Results and discussion

3.3.1 Circular motion around particles on agar surface

Our experiment starts by adding a tiny droplet of water (2-5 μL) next to a swarming colony, which causes some swarming bacteria to break away into swimming (see Sample preparation; illustrated in Figure 3.1a). This procedure allows us to select actively motile cells, usually seen at the swarm fronts. In a previous study on *E. coli* [26], the authors also focused on the edge of the swarming colony to select cells transitioning from swarming to swimming motion. We note in our experiment that a number of bacteria leave their pack at the swarm front and disperse over the agar surface (Figure 3.1b). As the droplet of water evaporates, most bacteria get stuck to the surface (in $\approx$ 1 minute) and cease the swimming motion. However, graphite particles or silica beads settled on the agar surface entrap a layer of water in their surrounding regions, allowing a few bacteria to swim around them, exclusively in clockwise trajectories (Figures 3.1c and 3.1d). Such an orbiting motion lasts over 10 min during observation, much longer than expected for a water film a few micrometers in thickness to disappear due to evaporation, as assessed later in the section.

We observed common orbiting motion among a wild type strain of *E. coli* (HCB33) and three recently isolated strains of bacteria, including two novel enterobacter isolates, SM1 and SM3, and one *E. coli* isolate, H5 (details in Materials and Methods). For the two *E. coli* strains, we used 0.5% agar containing added surfactant Triton X-100 (Sigma-Aldrich) of 0.1% vol/vol in order to facilitate the colony spread, making it easier to select active cells from the colony border. It should be stressed, however, that shallow tents of fluid around the micron-sized particles were observed in both cases with or without surfactant added into

the agar. *Enterobacter sp.* readily swarms on the agar gel without additional surfactant, which was the condition for the majority of our experiments. We also experimented with *Pseudomonas aeruginosa* (PAO1) and *Bacillus subtilis* (3610). In these two cases, we also noticed long-lasting water layers around the micrometer-sized particles where bacteria were motile. For *P. aeruginosa*, we observed orbiting around the micro-sized particles, but the motion was less organized. The motile cells near the particles tended to go off track from their orbits within a few seconds, possibly due to this species of bacteria frequently reversing flagella motor rotation direction, with a characteristic transit time of 0.56 s [2]. *B. subtilis*, which are longer cells (4-10 μm in length) remained motile within the water meniscus, but they did not orbit persistently. Instead, their maneuver appeared severely constrained by the small regions of the shallow film. These results suggest a common mode of motion of bacteria entrapped around microsized particles on moist surface, although the exact trajectories and maneuverability are species dependent. From here on, we focus the remaining report on *Enterobacter sp.* and *E. coli*, which reliably form circular trajectories.

3.3.2 Effects of particle size on the radii of meniscus region and bacterial orbits

Small graphite particles (< 2.5 μm in size) are usually not surrounded by swimming cells, possibly because they could not retain the water reservoir large enough to entrap bacteria. Large graphite particles (> 12 μm in size) retain liquid in a region over 40 μm in radius and thus keep many bacteria swimming in their proximity. Intermediate graphite particles were frequently seen to be surrounded by a few active swimmers and were the ones around which the orbiting of bacteria was most often observed and measured (Figure 3.1 d). In cases where the number of swimmers around a dispersed particle is big (over a dozen, as is commonly seen around large graphite particles or particles immersed in a dense bacterial population), the cells frequently bump into each other, making it difficult to discern individual trajectories. We chose silica beads of uniform size (4.5 μm in diameter) to perform the same experiment and observed equivalent results between the beads (Figure 3.2a) and

the graphite particles of comparable size, suggesting that the key parameter is the particle size, not its exact shape, nor its chemical nature. The common role of the graphite particles and silica beads is to sustain a tent-shaped water reservoir around them. We also observed for *E. coli* that they do not tumble as frequently when compared to bacteria grown in bulk liquid, a result reported previously for similar swarming colonies [45].

Around the particles where bacteria were observed to orbit, the radii of meniscus and bacterial trajectories both correlate to the particle size (Figure 3.2 c,b). The general trend is that bigger particles create taller water tents and of larger radius of meniscus, and the motile bacteria in the tent tend to move in larger orbitals before they are constrained by the meniscus boundary. Accordingly, we see a clear correlation between trajectory radius and meniscus radius, with the latter setting the upper limit, as shown in Figure 3.2b. For the silica beads, which are uniform in size, the meniscus and trajectory radii vary within narrow ranges. Graphite particles, which were more variable in size and had irregular shapes, gave rise to larger variation in meniscus and trajectory radii (Figures 3.2 b-d).

3.3.3 Causes for the circular trajectories and hydrodynamic analysis

The orbiting bacteria were observed to be in the same focal plane as the bacterial cells stuck in the nearby dry regions, suggesting the solid confinement imposed by the agar surface to be a key factor for the circular trajectories. Numerous previous studies have shown that bacteria swim in circular trajectories near a solid surface[23, 24, 44]. Such a hydrodynamic effect is expected to be strong in this experiment due to close proximity of the cells to the agar surface. Here, however, the trajectories are also subjected to additional constraints imposed by the tent-shaped film, especially the meniscus radius as its boundary cutoff. These constraints appear strong enough to keep the entrapped bacteria swim persistently in circular trajectories. In contrast, the boundary effects due to graphite particles on the bacterial trajectories may be neglected with exceptions of close encounters. In some cases bacteria were seen to swim within a body length from the center particle or occasionally

to even collide with it, but most often orbiting bacteria swam over 8 μm away from the particle, a distance by which the hydrodynamic effect of the graphite boundary becomes negligible [22]. These observations reinforce the argument that the circular trajectories are caused by the proximity of the bacteria to the agar surface and the meniscus boundary, but not the particle surface.

Measurements on all four strains show a common trend between the speeds of the orbiting bacteria and the radii of curvature of their trajectories. Bacteria swam slower in trajectories of smaller radii, but beyond a certain threshold ($\approx$ 7 μm) the speed approached an upper limit, between 30-50 μm/s, depending on the bacterial strain (Figure 3.3 a). These results suggest that graphite particles or beads affect the swimming speed by restricting the bacteria to their close proximity via the tent-shaped liquid film around them. Within smaller trajectories, bacteria cells are more restricted when compared to those that interact only with agar surfaces. Under such conditions the meniscus may push the cells closer to the agar surface, making them experience more drag and hence slowing them down.

We compare the experimental speed profile with predictions based on a hydrodynamic model by Lauga and co-workers [44]. Details on its implementation are described under the "Hydrodynamic model" section. Although it is possible to shift the theoretical line in Figure 3.3a by adjusting the parameters for the dimensions of the model bacterium and the flagellar motor rotation speed, the key feature remains the same: the speed initially increases with the radius of curvature, but quickly attains an upper value. Bacteria swimming at the lower end values of the radius of curvature moved closer to the seeding particle, hence they experienced more drag. This drag effect due to the seeding particle is not considered in the hydrodynamic model, which may explain why the data at radii of curvature below 7 μm fall significantly below the model prediction. The theory curve ends at radius of curvature $\approx$ 4 μm, which corresponds to a 5 nm minimal gap set in the model calculation between the cell body and the bottom surface (See Figure B.1). One might argue that the hydrodynamic model is no longer valid down to such a small gap. Nevertheless, the

consistent trend of the data with the theoretical prediction (Figure 3.3b) support the notion that whereas hydrodynamic boundary effect of the bottom surface can account for the circular motion observed in the orbiting bacteria, the actual trajectory radius and swimming speed are also affected by other constraints, such as those imposed by the particle surface, air-water interface, and meniscus boundary.

A more rigorous hydrodynamic model should include the air-water interface above the thin film. The boundary condition on the top surface may be modelled as free flow instead of non-slip. In fact, the free flow condition on the upper boundary would result in circular swimming trajectory of the same handedness as that caused by the solid boundary at the bottom. However, the boundary effect of the air-water interface could also be complicated by increased surface viscosity [46][47][48], for instance, due to adsorption of nutrient molecules initially contained in the agar. In light of this uncertainty, and our microscopy observation confirming that the bacteria tend to move much closer to the bottom surface, our hydrodynamic model has ignored the air-liquid interface, which is expected to contribute a smaller effect. As a side note, one useful outcome of this model is it confirms, based on the observation that *Enterobacter sp.* move in the same clockwise direction as *E. coli*, that both species of bacteria have flagella of left-handed helical structure.

3.3.4 Endurance of the water layer around the seeding particles

One key finding of our study is that graphite or bead particles on the agar surface retain a layer of water around them much longer than expected on a non-permeable surface. The evaporation of a water layer from a borosilicate glass surface containing microspheres (polystyrene beads of 6 μm diameter) on top has been investigated experimentally using x-ray transmission microscopy [42] . The full process lasts about 12 seconds, with 96% of the time on a pinning stage when the water film surrounding the bead thins gradually, and the last 4% on depinning of the water meniscus around the microsphere in the form of a sudden collapse. In our case, however, the fact that the bottom surface is made by agar

gel ($> 97.5\%$ water) allows for water to constantly permeate the upper surface. Thus, the meniscus lasts much longer. This observation is explained as a balance between evaporation and additional water pumped from the agar gel to the layer, as illustrated in Figure 3.4. Given the tiny thickness (a few μm) of the water layer, its internal pressure P is roughly constant everywhere. The internal pressure within the water layer (P) is lower than the atmospheric pressure P_o [16]. The difference between these two pressures is given by the Young-Laplace equation, $P_o - P = \sigma/R$, where σ is the water surface tension and $1/R$ is the meniscus curvature (only significant in the radial direction). Near the top of the agar gel, the pressure is also close to the atmospheric pressure. Hence, a pressure gradient is established between the permeable agar gel and the water layer, giving rise to water being pumped, as expected from Darcy's law [49]. Consequently, even though water is constantly evaporating from the thin layer, it is being replenished by that permeated from the agar gel.

To quantify the rate of evaporation, we exposed an open agar plate of 10 cm diameter to ambient temperature (22 degrees Celsius) and humidity (40%) and measured ≈ 0.5 gram weight loss per hour. This translates to ≈ 0.02 μm/s for the rate of water layer thinning. The agar gel of several millimeter thickness can sustain this rate of evaporation for hours when uncovered, or days when properly covered. But the same rate of evaporation poses a serious challenge for microscopic imaging, especially for confocal imaging on much thinner gels even in covered plate.

Additionally, we estimated the order of magnitude of the radius of curvature of the meniscus at the air-water interface that could sustain a balance between evaporation and water pumping from the gel. The radius of curvature can be calculated by applying Darcy's law, taking the pressure difference as the ratio of water surface tension to the radius of curvature. We use the meniscus radius as the characteristic length, since the dimensions of the agar gel are much larger, in the Darcy's formula: $\Delta P = \eta L v_z/\kappa$, where ΔP indicates pressure difference, η is the water viscosity, L is a characteristic length and v_z is the pumping rate along the pressure drop, in our case approximated by the evaporation rate.

The permeability coefficient is represented by κ. Not knowing the permeability coefficient of our agar gel, we take for order of magnitude estimate the reported permeability coefficient for 2% agarose gel, which is 616 nm^2 [50]. The radius of curvature thus estimated is around 83 mm, much larger than the diameter of the tentlike fluid film. This result indicates that even the slightest curvature in the top fluid surface suffices to provide enough pressure difference in order to maintain the fluid flow required to stably sustain the fluid film.

3.3.5 Confocal imaging of the gel surface deformed by seeding particles

We performed confocal microscopy to evaluate the deformation on the agar gel caused by 4.5 μm silica beads. Although it is technically impractical to do the measurements in the same setup as for the bacteria swarms, due to the requirement of the gel thickness not much larger than 100 μm for optimal image acquisition. A consequence of this limitation is that the water meniscus as shown in Figure 3.4 lasts under a minute, preventing us from capturing the profile of the thin fluid film even when it was filled with tiny fluorescent beads. Instead, the confocal images were acquired at the moments when the gel had become much drier than that of thicker gels on which the other microscopy experiments were performed. In essence, the images shown in Figure 3.5 only help visualizing the extent of deformation under the silica beads after the liquid film surrounding the large beads has dried.

Image blurriness poses additional limitations to our analysis. This is a well known problem for z-resolution of confocal slices, which is partially alleviated by deconvolution. Nevertheless, the trend line going through the middle of the red fluorescent band (Figure 3.5 c), highlighting Nile red labeled gel surface, indicates notable deformation below the position of a large bead. The absence of signal in the green light channel confirms the absence of the smaller Dragon green beads, as the area was covered by only the large bead. The valley of about 1.3 μm in depth for the line along the red channel gives a rough estimate for the gel deformation due to the 4.5 μm bead. The upward edges around the void of the green channel output indicate that numerous small Dragon green beads packed around this

region, capturing the history of the meniscus profile, as illustrated in Figure 3.4.

3.3.6 Comparison and contrast with a similar recent study

Wakita et al. [51] investigated bacterial motion in a shallow circular pool formed by compression and removal of glass beads 50 μm in diameter close to the edge of a swarming colony of *B. subtilis*. They identified several types of motion for the bacteria within the circular pools, leaving as an open question the physical mechanism responsible for the resilience of these pools of liquid, which also reportedly lasted for over 10 minutes. We see our experiment similar to theirs from the point of view of bacteria residing in localized water films on the agar gel, but rather different in geometric construction of the water film. While in their case the bacteria become trapped within the pools caused by mechanical compression (or indentation), in our experiment the motile bacteria are trapped above a flat agar surface but within a thin film of water under a shallow tent. Nevertheless, the thin liquid films in both cases are persistent, as they are connected to a large reservoir of fluid contained in a permeable gel.

We would like to point out that the compression of the gel surface as described in [51] is most likely not due to the weight of the beads, but the meniscus surface tension, via capillary effect. Specifically, the weight of the titan barium type (specific density 4.2 $\mathrm{g/mL}$) glass bead 50 μm in diameter is 2.7 nN, the deformation caused by the beads weight on a 0.5% agar gel surface, of Young modulus $\approx 30\,\mathrm{kPa}$ [52], would only be about 47 nm, estimated based on the model described in [53]. In contrast, compression on the gel surface due to the surface tension of meniscus around the bead, i.e., the capillary force, is more significant. We assume roughly a 10 μm radius for the contact circle at the air-water interface around the bead of 50 μm diameter and a 10-degree angle for the meniscus slope, as illustrated in Figure 3.4. The net vertical force integrated over the circle is 0.79 μN, which is nearly 300 times larger than the beads weight. The gel deformation under this capillary force amounts to about 2 μm, comparable to what was observed in [51]. This

deformation also accounts for our observation that glass beads or graphite particles anchor firmly to the surface once the shallow water tents are established. Performing a similar calculation for the 4.5 $\mu\mathrm{m}$ silica beads used in our experiment, taking into account the corresponding specific density of 2.7 $\mathrm{g/mL}$ and integrating over an estimated 1 $\mu\mathrm{m}$ radius for the contact circle at the air-water interface, we obtain an estimated indentation of about 1.0 $\mu\mathrm{m}$. Such an indentation is predominantly a result of the force due to the surface tension of water. These estimates confirm that capillary force, not gravity, accounts for significant compression on the agar surface by beads of only a few microns in diameter, as shown by confocal imaging (Figure 5).

3.4 Conclusion

In summary, we report a novel mechanism by which micro-sized particles on a moist surface entrap a tent-shaped layer of liquid within which flagellated bacteria swim in circular trajectories. The phenomenon occurs due to strong surface tension at the liquid-air interface and the proximity of the cells to a semi-permeable agar gel. Our findings indicate the potential for persistence of bacteria mobility in thin films of water. The observation that small particles can entrap bacteria under those conditions and allow them to remain viable and motile, even after the liquid film has evaporated from most of the surface area, is significant in certain environmental situations. For instance, this report helps reinforcing proper hygiene habits to prevent bacterial contamination, by keeping surfaces dry and clean, ideally free of particles, which might trap bacteria [54].

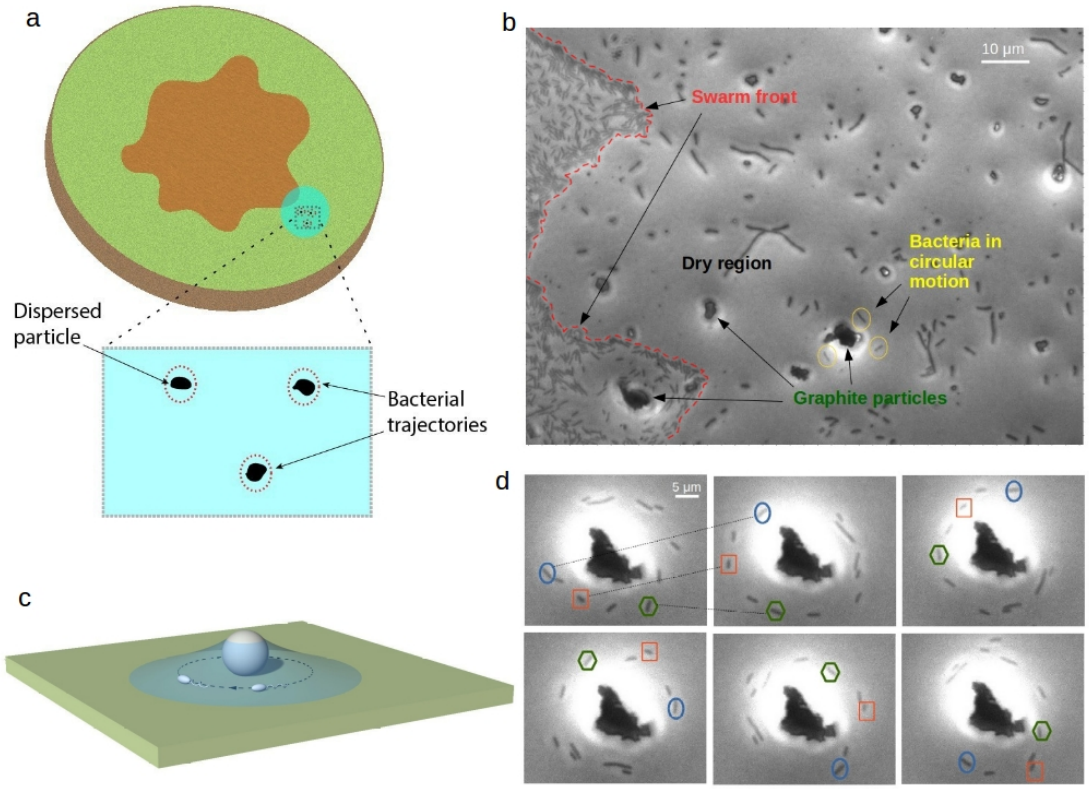

Figure 3.1: Circular motion of bacteria around particles on agar surface. (a) Schematics representing a bacterial swarm (in brown) with a water droplet (containing graphite particles or silica beads) added to a location overlapping the swarm front. A region in the droplet is amplified to illustrate bacterial trajectories around the dispersed particles. (b) Micrograph showing different features following the water droplet evaporation. The swarm front is marked by the red dashed line. Most of the region beyond has dried and is populated by bacteria stuck to the surface, except for those around graphite particles. (c) Artistic representation of bacterial cells moving around a dispersed particle within a tent-like layer of water around it. (d) Time lapse following the trajectories of bacterial cells orbiting a graphite particle. Three cells in particular are highlighted with different colors and geometrical contours to aid visual tracing. The sequence goes from left to right and the pictures shown were taken approximately 0.47 s apart.

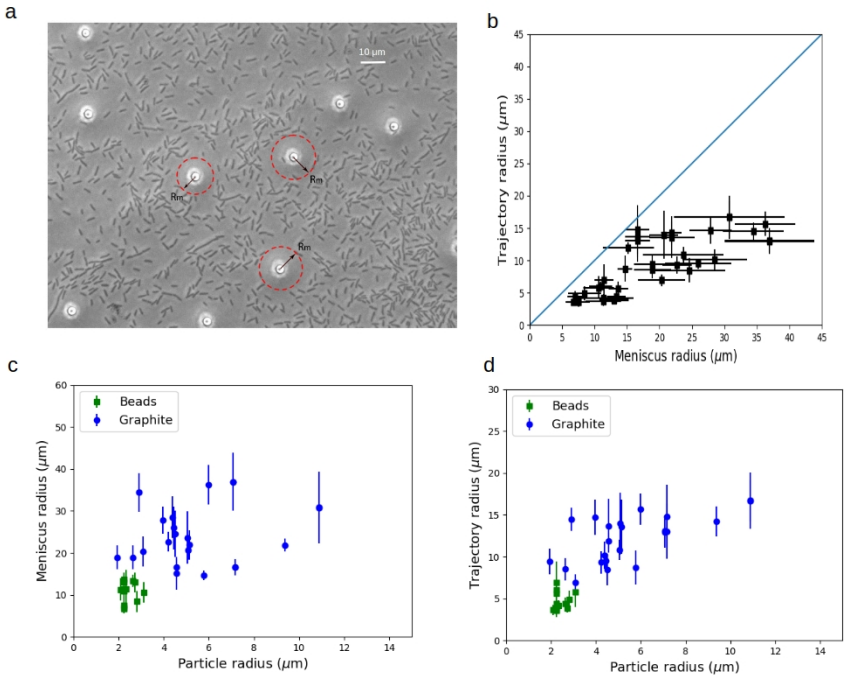

Figure 3.2: Image with meniscus of water layer indicated and plots of the measured dependence between meniscus and trajectory radii and particle size. (a) Micrograph highlighting the meniscus edge of water (radius Rm; defined in Materials and Methods under ”Imaging, measurements and graphic illustration”) around silica beads. Bacteria outside these circles are stuck in dried regions, whereas a few bacteria within these circles orbit around the beads. (b) Relationship between the cutoff radius of the water meniscus around the dispersed particles and the trajectory radius for bacteria orbiting these particles. The blue diagonal line of 45 degrees is a visual guide, which confirms the expected observation that the trajectories are confined within the meniscus. This plot includes orbits around both beads and graphite particles. (c) Relationship between the size of dispersed particles and the cutoff radius of their surrounding water meniscus. Each data point is an average over 5 measurements (see Materials and Methods for details on how these measurements were made). (d) Relationship between the size of the dispersed particles (graphite or beads) and the radius of trajectories of the orbiting bacteria averaged over three complete orbits around the seeding particle. In (b), (c) and (d) the error bars represent standard deviation. In (b) the error bars are shown in both x and y axes.

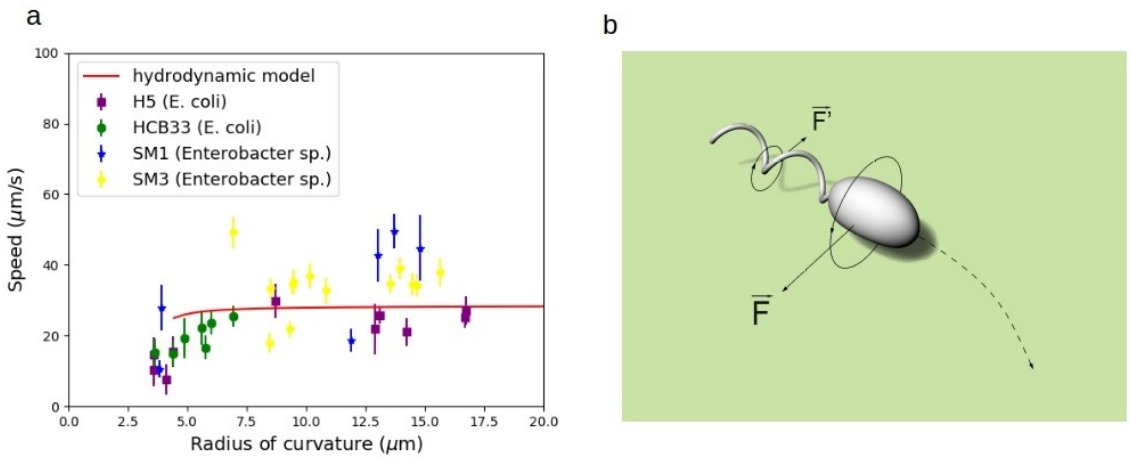

Figure 3.3: Measured speed versus radius of trajectory in comparison with numeric prediction by applying a simple hydrodynamic model. (a) Speed of bacteria with respect to the radius of curvature of trajectories for the four strains tested. The red line is the prediction by applying Resistive Force Theory (with parameters specified in "Hydrodynamic model"). The lower end of the line is set by the 5 nm minimal gap chosen between the cell body and the bottom surface in the model. Each data point represents measurements for an individual bacterium. (b) Schematics showing the curvilinear trajectory of a bacterium when it swims close to a solid boundary. The cell body and its flagellar bundle rotate in opposite directions. The larger drag on the cell body at the location facing the surface exerts a lateral force in the opposite direction to that on the flagella (forces indicated in the figure). The net torque leads to a circular trajectory.

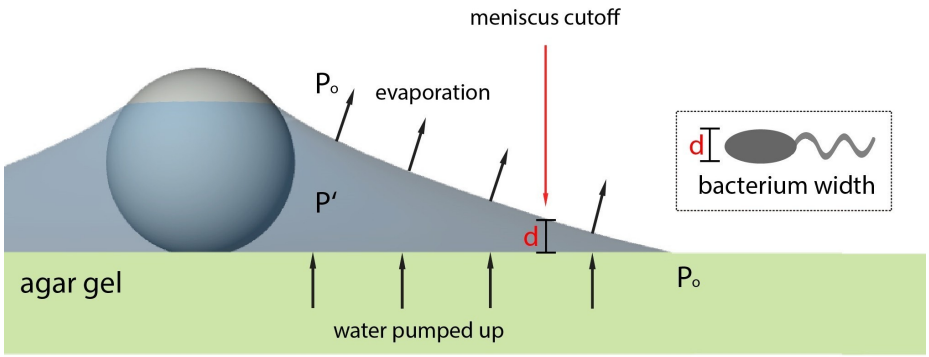

Figure 3.4: Schematics illustrating a resilient water layer around a micron-sized particle on an agar gel. The internal pressure (P) within the layer of water is lower than the atmospheric pressure (P_o), which is also roughly the pressure inside the agar gel close to the top surface. This pressure difference pumps water up from the semisolid agar gel, counterbalancing constant evaporation. Hence, the water layer is maintained much longer than on typical non-permeable solid surfaces. The thickness d corresponds to the width of a bacterial cell, with its location defining a meniscus boundary outside which bacteria get stuck to the agar surface. Note we have ignored the deformation on the agar surface due to the bead, which is discussed in the text.

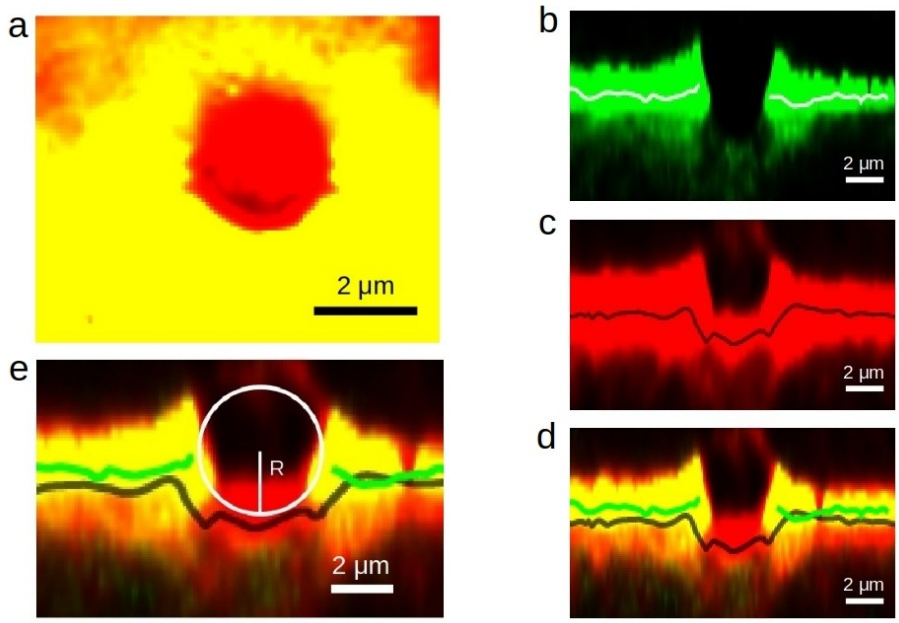

Figure 3.5: Confocal microscopy images illustrating a small but notable compression of a 4.5 µm bead on a 0.5% agar surface. The surface is covered by much smaller beads of 0.5 µm diameter labelled in Dragon Green, which is excited by blue and green lights to emit green and red lights, but with green the strongly favored emission. Additionally, the gel is also labeled with Nile red, which is mainly excited by green light, emitting red. (a) top down view of a single confocal image slicing through the center of the bead. Yellow light comes from merging green and red channels. The red circular region indicates the presence of the 4.5 µm bead due to the absence of green. This is because the smaller Dragon green beads were precluded from the site. (b), (c) and (d) represent an orthogonal cross-section of (a) when opening the green channel (b), the red channel (c), and both green and red channels (d). The trend lines in these images indicate the middle line through the bright band. The absence of green light signal in the middle of (b) indicates the absence of Dragon green beads in that region. Presence of a deformed red region in (c) shows a somewhat compressed surface of the agar gel. (e) shows (d) with an illustrative circle, indicating where the bead sits.

CHAPTER 4

ASSESSMENT OF TRANSIENT BACTERIAL ATTACHMENT TO A SOLID SURFACE BY APPLYING AN ELECTRIC FIELD

4.1 Introduction

Ubiquitous in nature, bacterial attachment to surfaces has been widely studied [55, 56, 57]. To human and animal hosts, bacterial attachment is often the first step towards infection [58]. Attachment is also the most crucial step for the formation of biofilms, which may also involve other triggers such as fluid flow [59]. In the process of exploring their environments, bacteria often encounter solid boundaries. In spite of swimming motility and Brownian motion [24], motile bacteria tend to accumulate near interfaces [21, 19]. When within 2-3 μm from a surface, they may become sterically or hydrodynamically trapped and remain in the proximity of the surface for significant lengths of time [22]. Although distinct from attachment or adhesion, near surface accumulation and entrapment help facilitating bacterial attachment.

Attachment to surfaces can be classified according to its molecular basis, as well as strength and reversibility. Most bacterial species attach and adhere to surfaces via special appendages such as pili, which have been extensively studied. The attachment by pili and their retraction are known to lead to strong and permanent attachment. Less is known, however, for other forms of attachment, particularly those weaker and more reversible, even though they play functional roles. For instance, weak and reversible adhesion has been shown to enhance surface colonization [60]. Sequences of attachment and detachment of binding tethers may serve as pre-play in the process of consolidating irreversible attachment [61]. These transient attachments are also linked to optimal surface exploration as it has been proposed to maximize bacterial surface diffusivity [62].

Bacterial colonization of a surface can be undesirable, such as in formation of dental plaques and various types of bacterial infection [63]. As a consequence, different techniques have been applied in order to remove bacteria from surfaces, for example, by flow, through the passage of air-bubbles [64] or by applying electric field on conductive surfaces [65, 66]. In the last case, it was observed that electric forces parallel to the surfaces are more efficient to promote detachment than those applied in the perpendicular direction [67]. However, there has not been much study to systematically apply electric field in order to quantitatively assess as a means of investigating bacterial attachment to surfaces.

We chose a Gram-negative bacterium called *Caulobacter crescentus* as a model system for the study of bacterial adhesion. Commonly found in aquatic medium, including soil and drinking water [68], *C. crescentus* has a dimorphic life cycle: One newly divided cell is motile and called a swarmer, which in about 45 minutes develops into a stalked cell. Under favorable conditions, the stalked cell can proceed to the next division, producing a motile swarmer cell as its offspring in every two and half hours [68, 69]. The stalked cell is known to produce a holdfast capable of strongly and permanently adhering to a solid surface [70]. However, initial attachment in most laboratory based adhesion study of *C. crescentus* tends to occur early in the swarmer stage. Effective attachment to surfaces for this species is aided by the presence of type IV pili and flagellar motility [71]. In fact, the swarmer attachment has been shown to trigger just in time expression of holdfast and accelerate the swarmer cell to stalked cell transition [72]. Aside from strong adhesion and permanent attachment via its holdfast facilitated by pili, We focus in this work on mutants that lack pili, in order to study weak attachments involving other surface molecules or mechanisms. A recent study on the tethered motion of *C. crescentus* swarmer cells of the same strain suggests ”fluid joint” possibly formed by polymers on the cell surface [73]. In addition, it has been reported that the curved shape of *C. crescentus* may help the cell to colonize surfaces [74].

In this study, by applying electric fields parallel to a plastic surface, I perform exper-

iments based on the initial observation that some weakly attached cells are readily detached while others remain stuck to the surface. More interestingly, a small number of tethered cells exhibit transient characteristics of moving slowly along the surface, driven by the field, but never leaving the surface proximity. These particular cells move at erratic speeds. They alternate between being mobile and tethered. We refer to this phenomenon as *quasi-attachment*. This chapter focuses on this peculiar behavior and suggests a molecular mechanism for it.

4.2 Materials and Methods

Two strains of *Caulobacter crescentus* were used in this study: CB15 ΔPilin (provided by Yven Brun when he was at Indiana University) and SB3860, which is a mutant derived from CB15 ΔPilin (kindly generated by Bert Ely from the University of South Carolina, Columbia). Both bacterial strains lack pili, making them less likely to adhere to surfaces. SB3860 only swims forward.

Caulobacter crescentus was grown in PYE (peptone yeast extract), followed by a synchronization method [72] in order to select swarmer cells. The culture containing primarily swarmer cells was diluted in DI water, in a proportion of 1:3, and the mixture was inserted into a microscope slide containing a capillary channel (μ-slide I luer from *Ibidi*, Munich, Germany), as illustrated in Figure 4.1. The channel dimensions are: 50 mm in length, 5 mm in width, and 0.4 mm in height.

Both ends of the channel were sealed with agarose gel (0.5 % in weight of agarose in a 50 mM Na_2SO_4 solution). Specifically, agarose mix in liquid state was gently deposited at one end of the channel previously filled with the bacteria containing liquid. The slide was gently tilted to aid the gel mix to enter the channel by a millimeter or two. After a 2 minutes wait for the gel to solidify, agarose mix was filled to the other end of the channel, resulting in both ends of the capillary to be sealed by the agarose gel (see Figure 4.1 for channel visualization). The agarose gel prevents electrochemical products at the

electrodes from spreading into the channel, adversely affecting the bacterial behavior. The agarose seal on both ends of the capillary also efficiently limits the fluid flow within the capillary. In addition, the surface of the type of capillaries we purchased is hydrophobic, which essentially suppresses electro-osmotic flow. As a result, we noted no obvious flow near the surface when the electric field was applied during the course of our experiment.

The electrodes were made of gold (99.99% purity, from Sigma-Aldrich) which is an excellent conductor. This concern with sealing the channels with agarose gel and choosing an inert metal came from the observation that the products of chemical reactions happening at the electrodes are harmful to bacteria and a less restrictive setup had the potential to kill most bacteria within a few seconds under applied voltages over 50 V. DC voltages up to 120 V were provided by a power supply (CSI12001X, Circuit Specialists, Tempe, AZ). We noticed that applying voltages over several minutes would still cause cracking of the agarose gel near the electrodes, where chemical reactions occur. As a consequence, bubbles were produced in these regions, which altered the electric current. To avoid this adverse effect, most of our experimental data were acquired within a few mins following an applied voltage.

Electric currents were measured by adding a amp-meter (DROK, China) in series to the circuit. Upon application of an electric field, the capillary channel behaved as a non-Ohmic conductor as the relationship between voltage and current appeared nonlinear (see Supplementary information). We also noted that the measured current increased over time, perhaps due to the electrochemical effects. Applying higher voltages ($>$ 100 V) for longer period of time led to even higher electric currents. The nonlinear behavior of the measured I-V curve may be attributable to our order of measurements ramping up sequentially from lower to higher voltages.

Images were acquired using phase contrast under a upright microscope (Eclipse E800; Nikon) with 4x or 40X objective lenses (Nikon) and recorded with a charge-coupled device camera (Coolsnap EZ; Photometrics). The acquisition process was controlled using Meta-

morph software (Molecular Devices). The frame rates for video recordings were 33.88 or 9.96 frames per second (fps). For image processing, particles were tracked using ImageJ and AItracker, an artificial intelligence particle tracker based on neural networks [75]. The bacterial trajectories which were used in the velocity calculations shown in Figures 4.4 and 4.5 were processed using a third order Savitzky- Golay filter with window length of 5. This step allows the experimental data to be smoothed, filtering some noise, but keeping its fundamental features.

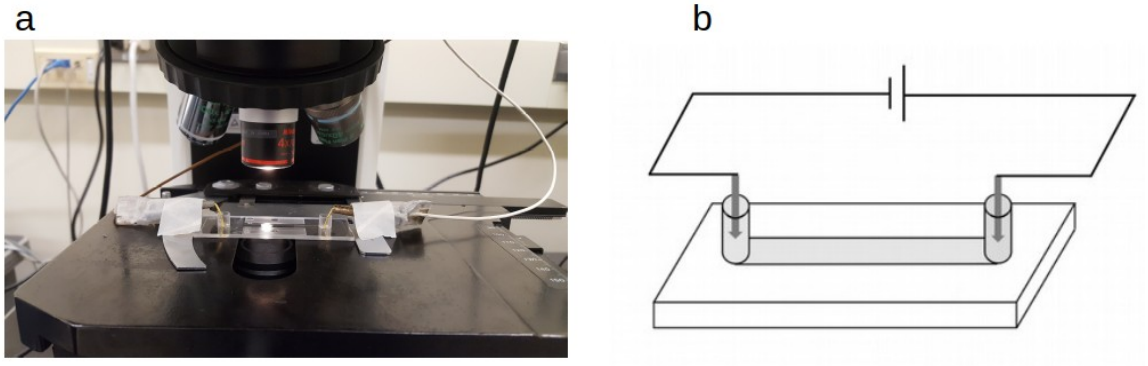

Figure 4.1: Experimental setup. a) Picture showing a sample slide on a microscope stage. Two wires are connected to electrodes placed at both ends of a capillary filled with the bacteria. The microscope slide is fixed so that a part of its capillary channel is imaged while an electric voltage is applied. b) A simple sketch of *a*.

4.3 Results

4.3.1 Alignment of trajectories under an electric field

Once exposed to an electric field, the effect of galvanotaxis for bacterial motion is immediately observed. In the absence of external electric field, the swarmer cells of *C. crescentus* swim in random directions, which change in the time scale of seconds (Figure 4.2a). The applied electric field imparts a drift speed on every bacterium, motile or not, but the effect on swimming cells is more dramatic as the field has aligned their swimming trajectories. The average direction of motion is opposite to the direction of the electric field, indicating negative net charge of the bacterial cell. The alignment in trajectory is mainly caused by

orienting the cell-flagellum axis, with the cell body heading towards the positive electrode and the flagellum pushing from behind in most cases. This observation suggests the cell body is more negatively charged than the flagellum, and the ratio of the electrophoretic driving forces on the body and tail is larger than that of the hydrodynamic drags on them. Under stronger fields, the paths of motion become closer to long and straight lines that are nearly anti-parallel to the field direction (Figure 4.2b).

It is interesting to note that some cells are observed to swim in the direction of the field, i.e. towards the negative pole, typically at much slower speeds. This observation suggests that in these cases the swimming direction is parallel to the electric field, driven by its flagellum pulling the cell body backward. With natural variation in motor torque, for some cells this backward swimming motion appears to have overcome the electrophoretic effect, resulting in net slow motion down stream with respect to the electric field. In the absence of electric field, *C. crescentus* switches the direction of swimming within a few seconds [76] (unless genetically modified to prevent such a behavior, such as SB 3860 strain, which swims solely forward). I indeed observed switches under the applied field, but a randomly large change in the direction of motion as the result of a flick [3] became less evident. Even with the changes in direction of motion, the trajectories remained mainly aligned with the electric field. One example is shown as trajectory 5 in Figure 4.2b. This alignment behavior is not specific to *C. crescentus*: our limited experiments with *Pseudomonas aeruginosa* showed similar results. In short, immediate and large changes in trajectories of swimming bacteria under an applied electric field can be accounted for by analysis of flagellum propulsion, field alignment, and electrophoretic forces.

4.3.2 Types of motion under an electric field

Under an electric field, four different behaviors were observed for individual cells: 1. Non-swimmers, including possibly dead cells, just drifted towards the positive pole, due to the electrophoretic force caused by the electric field. 2. Cells that remained nearly immo-

bile for some time, at most giggling about their fixed positions due to Brownian motion. Some of these cells were seen to be spinning at fixed positions before the electric field was applied, an indication of surface attachment mostly through body or flagellum tethering. 3. Swimmers which kept their swimming motion, either against the direction of the field (more often) or opposite to it. 4. Cells, which initially attached to a solid surface, moved along the field, but slowly and with highly variable speeds over time. I interpret such a behavior as alternating between transient motion and surface attachment. I define this transient attachment as "quasi-attachment". Figures 4.3 a,b highlight examples of this behavior, as well as cells that are permanently attached to the surface. While free swimming cells quickly move away from their initial positions, the motion of these slow cells is more constrained, as indicated in Figure 4.3.

4.3.3 Speed variation of transiently attached cells moving under the field

I noticed that the free swimmer cells, when moving against the direction of the electric field, tend to move faster as the field strength is increased, as expected. In contrast, the slowly dragging cells behave differently. These cells frequently drop their speeds to negligible values. They transit from short moments of limited mobility to moments of attachment to the surface, an example of which is shown in Figure 4.4 b. During the short intervals when the cell was moving, its velocity component along the field axis remains highly variable. It is possible that this noisy speed-time curve was also due to very brief moments of attachment, but we could not definitively show that since all speed data were averaged over about one tenth of a second set by the frame rate of the images taken.

One surprising behavior of these dragging bacteria is that no obvious correlation is noted between the intensity of the applied field and the moving speed of the cells. Figure 4.5 shows six examples of averaged velocities along the electric field axis from dragging cells (strains CB15 $\Delta Pilin$ and SB 3860) under different electric fields. There is a large variation in each cell's moving velocity over time, as indicated by the large error bars

representing the standard deviations. The average velocity also varies among the 6 cells, but there is no obvious correlation between the average velocity and either the voltage applied or the strain of the cells tested. Note the trajectories of these cells are aligned with the field axis. Thus the velocity component properly accounts for the average drift velocity of these transiently attached cells.

4.4 Discussion

4.4.1 Charge distribution along the bacterial cell is primarily responsible for trajectory alignment

One simple explanation for the alignment of bacterial trajectories under an electric field is that there is a difference in electrophoretic mobility of the cell body and that of the flagella filament [77]. Whereas this explanation has been suggested for some multiflagellated species of bacteria, it may be extended to *C. crescentus*, as well. The typical area on the cell body is in the order of 2-5 μm^2 [78], which is around two orders of magnitude bigger than the surface area of the flagellum, whose averaged contour length is a few μm and thickness diameter about 14 nm [79]. The hydrodynamic drag on the cell body is also larger than on the much thinner flagellum. Based on our observation that motile cells swim rapidly towards the positive electrode, faster than the speeds of non-motile cells, we know that the cell body usually leads the flagellum as the bacteria are both driven by the field and pushed by the flagellum towards the electrode of higher voltage. The experimental results also suggest that the ratio of the drag coefficient is much less than that of the effective charges between the two. The imposed cell orientation dictates the kinematics of the bacterial trajectories. Under strong fields (with applied voltages above 40V in our experiments), cell trajectories do not deviate much from straight lines even for cases when we observe switches in the direction of motion. This result is partially due to alignment of the electric field, but possibly also partially due to suppression of flagellum flicks [80]. A flick occurs when a uniflagellated bacterium changes from backward to forward (cell body

forward) motion. For *C. crescentus*, with its flagellum of right handed helical structure, a flick occurs as its flagellar motor switches rotation from counter-clockwise to clockwise. Whereas a flick often causes the bacterium to reorient its cell body orientation, causing a large change in swimming direction, the presence of a strong electric field keeps the cell body aligned, thus suppressing the flicks even if switches in motor rotation directions is unaffected.

4.4.2 Cell surface polymers may be the cause for the transient attachment to a solid surface

To my knowledge, there is currently no definitive explanation for how bacteria make transient attachment to surfaces. It has been proposed [73] that a "fluid joint" made up of polysaccharrides that cover the cell wall could be responsible for the interaction with the surface (Figure 4.6). The tether region seems to be located near the flagellar pole in most cases, but occasionally also near the center of the body [73]. Given that the nature of this cell-surface attraction is proposed to be caused by polymeric bonding between the bacteria wall and the surface, we suggest to refer this interaction as via *polymeric tethers*. The reason for this proposed change in terminology is that "fluid joint" implies no molecular link, but instead, the action of a thin layer of confined fluid. Along with the collaborators for this project, I hereby suggest explicitly in the sketch multiple molecular tethers, which logically accounts for the "quasi-attachment". A single, non-specific molecular interaction would unlikely be strong enough to withstand the applied field. Plus, if tethered by a single bond, its breakage would immediately set the cell free, leaving very low probability for repeated attachment. Although unable to visualize these polymers, we envision multiple tethers with multiple transient attachments, which best account for the large variation of the drag speed, while the cell remains continually attached. Additionally, since *C. crescentus* has a curved shape, as the cell is frequently going through moments of attachment and detachment, the region of cell-surface contact may vary significantly and hence the force of

attachment. The bonding at different locations on the cell surface could lead to variations in the speeds of motion for such a cell even if there is a constant force driving it to move parallel to the surface.

4.4.3 Comparison on forces of detachment with other methods

The method of applying an electric field to detach cells from a surface offers an unique attribute as compared with other techniques. In the experiment addressed in this chapter, the typical force applied is on the order of 0.1 pN (see supplemental material - Appendix B). Such a strength of force is 1-2 orders of magnitude stronger than achieved by the common micro-fluidic approach [81]. However, it is orders of magnitude smaller than those by laser tweezers (1-100 pN) [82, 83], atomic force microscopy (AFM) (order of nN) [84], or micromanipulation techniques (up to microNewton)[70]. The strength of bacterial adhesion have been shown to cover such a wide range of magnitudes spanning all these techniques. Interestingly, the present study shows that forces in the sub-pico newton range prove to be required to detach a pililess strain of *C. crescentus* that weakly and non-specifically attach to a plastic surface. Such weak and transient interactions might be significant prelude to much stronger and permanent bacterial attachment to surfaces. There has not been that many studies in this particular range of weak interactions, perhaps due to a lack of appropriate tools. To this end, the method shown in this study may prove useful for future studies on a variety of microbes in the context of their transient interactions with surfaces, including those under more environmentally or medically significantly settings.

4.4.4 Could flagellar filament cause transient attachment?

One alternative possibility is that the flagellar filament frequently scratches the solid boundary, causing too large a drag to allow fast motion of those cells touching the surface. Given that a typical flagellar rotation rate is on the order of 250-375 Hertz [85], the flagellum could be interacting with the surface with the high frequency on the order of hundreds of

times per second, imposing a strong drag on the bacterium. This interaction of flagellum and surface could also be a cause to the transient attachment. A potential method to test this hypothesis would be by directly visualizing flagellum. This method requires labelling the flagellar filament while not severely affecting the flagellated motion. One might then be able to directly visualize the behavior of the labelled bacteria when they undergo transient attachments under applied electric field. This approach has prove challenging previously, using genetically modified strains of *C. crescentus* so that its flagellum could be labelled. Unfortunately, the labelling resulted in much reduced motility and only in very few cases, short video segments showing in rare occasions a motile cell with a faintly labelled filament. Once a better improved labelling technique is developed, applying it to the experiments under electric field as described in this report could lead to better understanding to what extent the flagellar filament affects the transient attachment.

4.4.5 Other alternative hypotheses

One alternative hypothesis is that these slow moving cells are just cells that are swimming towards the negative pole, i.e. in the field direction, opposite to the electrophoretic driving force. In this scenario they would be moving slowly because they would be ”fighting” against the electric force. However, since the slow irregular motions are seen over dozens of seconds, whereas we know from an earlier study that the characteristic time for switching the direction of motor rotation rarely goes beyond a few seconds [76] (for $\Delta Pilin$ cells; SB3860 only swims forward). It would be very unlikely, based on this alternative picture, that a $\Delta Pilin$ cell would be swimming over 30 seconds in the same direction along the electric field. In fact, we observed multiple examples of slow dragging motion for $\Delta Pilin$ cells, thereby ruling out this alternative model.

Other alternative hypothesis can be considered, such as that the no-slip boundary condition for fluid flow might account for the transient and slow dragged motion. This picture is inconsistent with results from another earlier study measuring the swimming speed of

C. crescentus as a function of its distance from glass surface using total internal reflection fluorescence (TIRF) microscopy. We found the cells swim relatively freely as close as on the order of ten nanometers from the surface, with their typical swimming speeds 40 $\mu m/s$ [24]. The qualitatively different type of motion and the much slower and highly variable motion of the subset of cells identified in this study leave us with the most natural conclusion of "quasi-attachment", by "polymeric tethers".

4.5 Conclusion

We report on the observation of frequent and transient attachment and detachment of *C. crescentus* from a solid surface. The events were identified by applying an electric field parallel to the surface. These transient attachment, via "polymeric tethers", reinforce the idea of polymeric interaction between the cell wall and the solid boundary. Our analysis of these events of weak adhesion offers insights on the mechanism, as well as potential applications to remove bacteria from surfaces.

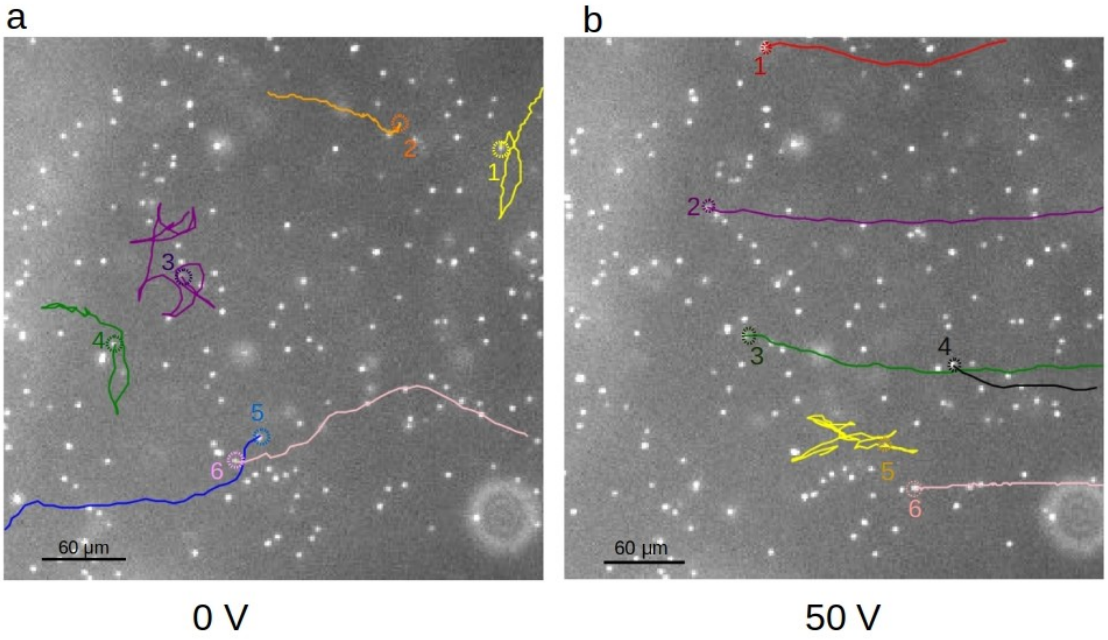

Figure 4.2: Bacteria trajectories. a) No electric field applied, the trajectories show random swimming directions and with changes in direction at random time. b) Under a 50 V voltage, bacteria move predominantly against the applied field. The direction of the field on the figure goes from right to left. The dashed circle on each trajectory indicates the starting point of the track. The bright dots are images of bacteria, most of which are motile. For clarity, only six cells are highlighted on each figure. Some cells move beyond the borders of the imaging area. The images were taken using a 4x objective lens.

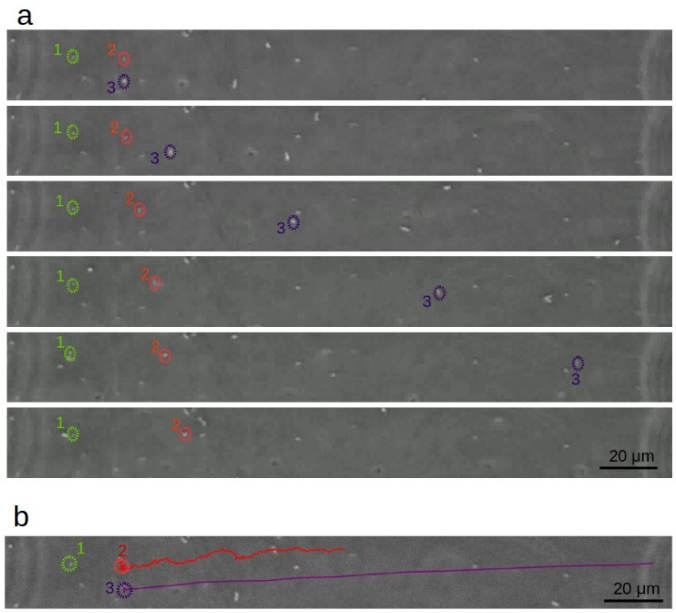

Figure 4.3: Types of bacterial motion under the electric field. a) Particle 1 is attached to the surface and hardly moves. Particle 2 moves slowly under the field, experiencing frequent transitions in speed. Particle 3 is initially attached to the surface, but it detaches quickly after the electric field is applied and moves fast and freely along its path. The images in the sequence are 2 seconds apart. b) Tracing the trajectories as illustrated in Figure a) over 31 seconds. Notice that the time interval traced is longer than for what is shown in the time lapse sequence in a). The images were taken using a 40x objective.

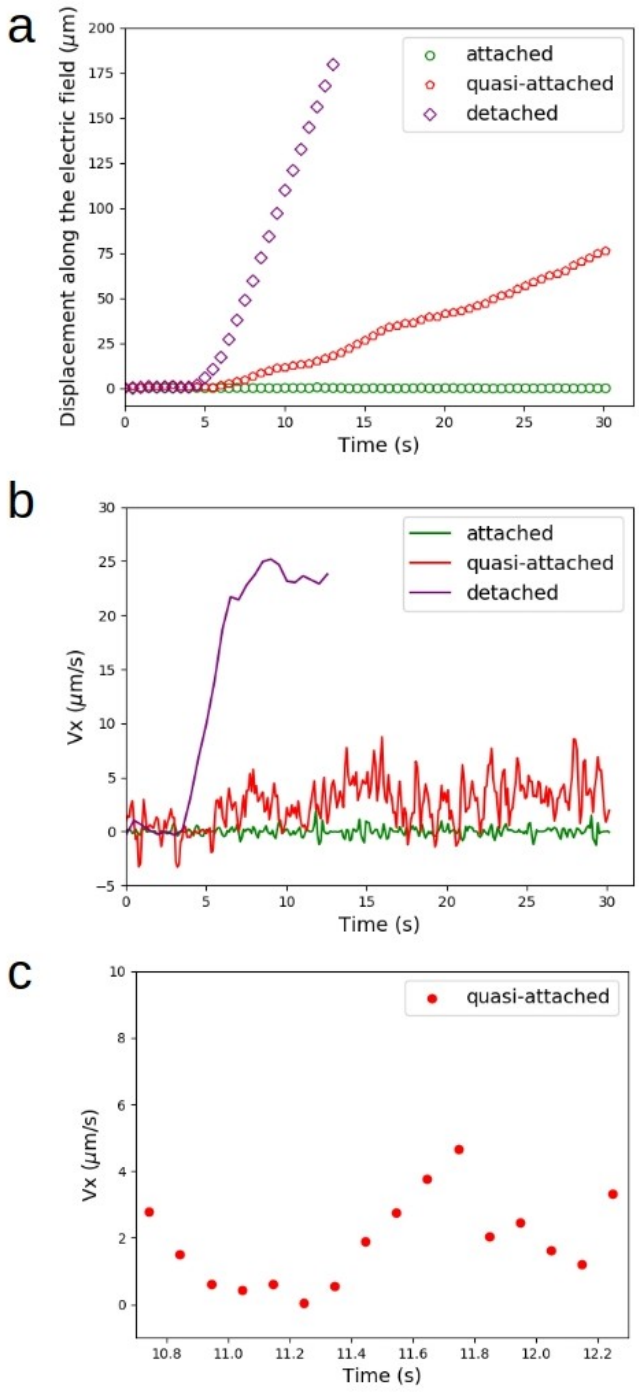

Figure 4.4: Displacement and velocity along the field measurements. a) Displacement of the highlighted cells along the axis of the electric field. Experimental data are shown for points separated by 0.5 seconds, which is five times the time interval for data acquisition. The voltage applied increases from 0 V to 100 V within seconds, and then remaining at its maximum value. b) Velocity along the field as a function of time for the three highlighted cells shown in Figure 4.3. c) Zoomed in plot of velocity values lasting approximately 1.5 seconds of the experimental data in Figure *b* above. Within this short time interval, we see in more detail the variation of velocity along the field. At the moment from 10.9-11.3 sec, the velocity is close to zero, indicating transient attachment.

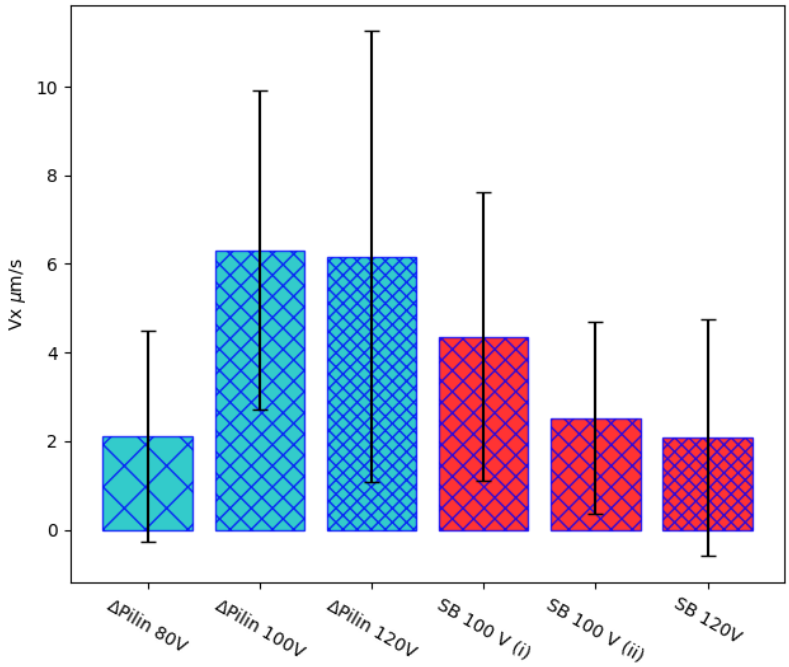

Figure 4.5: Average velocity component along the axis of the electric field for six dragging cells from two different strains and under different values of applied voltages. The error bars represent the standard deviations.

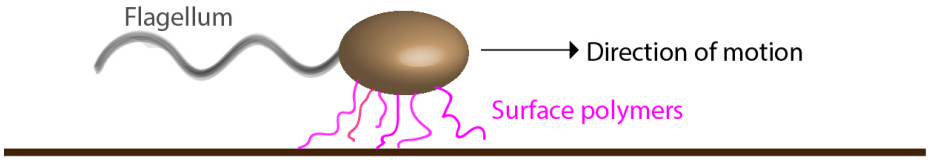

Figure 4.6: Illustration of transient bacterial attachment to a solid surface through polymers out of the cell wall.

CHAPTER 5
CONCLUSIONS

The results in this thesis are mainly divided into what were discussed in chapters 3 and 4. Both chapters employ bacteria as the experimental system of study, but under very different conditions. Other related studies, that are independent on their own, but came from the analysis of applying electric fields in capillary channels are briefly discussed in Appendices C and D. These side projects have the potential to be more deeply investigated in order to gain more insights into bacterial interaction with surfaces and the electrokinetic effects on micro and nano capillary channels.

Summary of results

In chapter 3, it was reported the finding of thin liquid layers around micrometer sized particles that were resilient to evaporation due to fluid replenishment coming from the gel water ”reservoir”. Looking from this point of view, bacterial cells acted as tracers for the fluid film. Bacterial motion or immobility allowed for the determination of the liquid layers, giving that the liquid itself is transparent and invisible in the microscopic observation. The motion of the bacterial cells was also intriguing to observe because of their orbital trajectories around the seeding particles.

Circular motion of bacteria near a solid boundary is not entirely new, although not in the same setup as the one shown in this study. Here, it was possible to have exquisite control over the radius of the circular trajectories as they correlated with the height of the seeding micro particles. An important feature of the phenomenon is the mechanism of essentially micro-pumps on the agar gel interface, driven by the Young-Laplace pressure caused by the curvature on the thin film surface. This mechanism acts to entrap motile bacterial cells over a 10 minutes time interval. Also, in the way the experiment was designed it leads

to the selection of the fastest cells on a swarming colony front. The fastest cells are the ones that reach the water pools further from the initial water droplet deposition before the water evaporates. Eventually, a similar method, which has minimal side effects on the cell's health state, could be designed for selection of viable sperm cells. Such an application is constantly sought in the livestock industry or human reproduction [86].

In chapter 4, I have described original observation and offered a molecular model for bacterial adhesion to solid surfaces in cells that lack pili. In particular, the experimental data show a transient attachment phenomenon in which the bacterial cells switch back and forth between detachment and attachment. The nature of this cell-surface interaction was attributed to a connection mediated by polymeric tethers, which may naturally extend out of the bacterial surface. Also, the alignment of the bacterial cells with an applied electric field indicated effective suppression of the flicking maneuver under this experimental setup.

In this study, the external electric field worked in the sense of removing or preventing bacterial adhesion to surfaces. This experimental design allowed for the observation and analysis of transient attachments. A full description of the nature of bacterial attachment to the surface will require higher resolution images, possibly resolving flagellar filaments by fluorescence labelling. Labelling the flagella while maintaining their propulsive active would also help explain the role they play in the dragging motion of the bacterial cells under the electric field.

Perspectives for future studies

Regarding the orbiting bacteria project, further studies could lead to potential applications or more in depth comprehension of the observations. For instance, the pumping rate of the agar gel caused by the deposition of graphite particles or microspheres was estimated based on the steady state balance with the evaporation of the water layer. A detailed investigation of the gel porosity or higher resolution images, such as with x-ray microscopy, would allow for a more quantitative result. Trying out the experiment with different gel compositions

could also better define its influence on the pumping rate. As a potential application, in addition to the fast cells selection, this experimental design shows a way to keep micro-sized material wet over extended periods in samples that are open to the air. The result is achieved without relying on a complex irrigation system, suggesting potential applications to systems similar to the one described in this study..

Likewise, the electrophoresis experiment with the dragging bacterial cells suggests a way to prevent bacterial adhesion to surfaces through the application of electric fields. A deeper understanding on the attachment mechanism would require better imaging of the cell-surface contact area. The effects of electroosmosis, for instance, could be better evaluated by working with glass capillary channels, which has a charged surface. Preliminary studies with ”home made” glass capillaries glued to a microscopy slide have indicated the presence of significant counterflow of cells near the capillary boundaries. These capillaries were not stable enough to produce best quality data, but the development of a more consistent method to fabricate these channels may overcome the data quality issue, allowing for rigorous investigation of electro-osmotic effects in such systems.

Appendices

APPENDIX A

SUPPLEMENTARY INFORMATION FOR CHAPTER 3

A.1 Estimating graphite heights

Here I describe the procedure to estimate the heights of graphite particles used in the experiments described in chapter 3.

Graphite particles obtained by scratching a pencil are highly variable in size. They tend to lay on the agar surface along their two longer dimensions. For convenience, I define graphite diameter as the square root of the product of the longest and the shortest axes along the particle imaged under the microscope. I also refer the particle diameter thus defined as its size, so that readers do not falsely imagine the particles to be spherical. By moving the fine knob in the microscope that controls the focus in the vertical direction, I estimate what is the height of the graphite particles. To calibrate this estimation, I also deposited a mixture of silica beads with well-defined dimensions (1.0 μm and 4.5 μm in diameter) and the graphite particles on the agar gel. Moving the knob from the position with the top of the bigger beads in focus to that of the smaller beads in focus I calibrate the translation of the knob with the vertical height. This calibration is applied to estimate the height of the graphite particles.

In order to assess the thickness of the liquid film around graphite particles where orbiting bacteria were observed, I made separate measurements for graphite height versus diameter. Although I did not measure the ones with bacteria orbiting, I measured particles within the same size range from the same preparation. One notes on Figure A.1 that, except for a few outliers, wider particles tends to be also taller. There is a wider distribution for diameter than height, which may be related to the layered structure of graphite and the fact that objects are more likely to sediment with their larger dimensions laying horizontally.

For example, when falling on the floor, a cell phone always lands with its face up or down, not on its side.

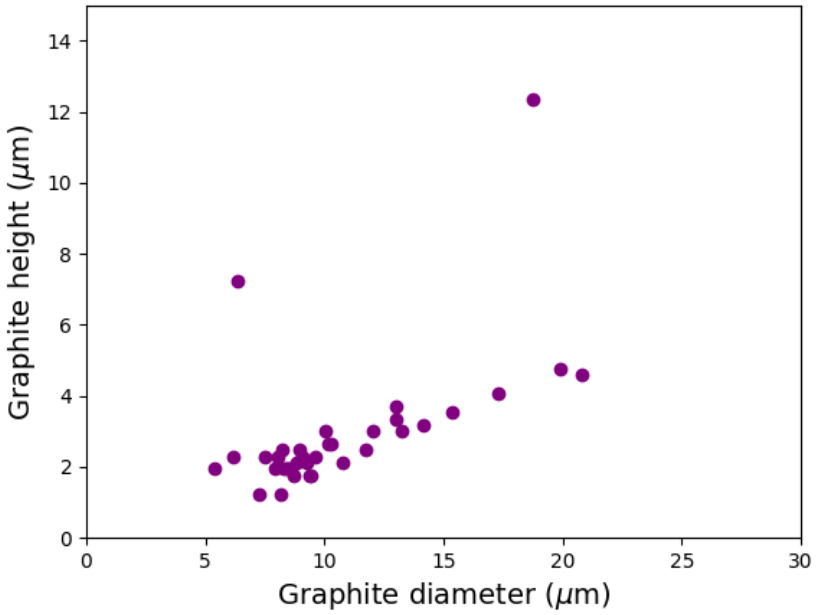

Figure A.1: Correlation between the height and the diameter of graphite particles. A scatter plot of graphite heights versus diameter for 36 particles with their size in the range in which orbiting bacterial motion was observed. A few data points in the diameter range of 7-9 μm were obscured due to overlap.

A.2 Resistive Force Theory numerical calculation

Table A.1: Parameter values used in the numerical calculations

Parameter definition	Value
Wavelength of helix: λ	1 μm
Radius of helix: b	300 nm
Radius of cell body: a	0.6 μm
Viscosity of medium: η	0.89 mPa.s
Width of cell body: w	1.2 μm
Rotation frequency of flagella: f	150 Hz
Rotation speed of flagella: ω	2πf
Number of wavelengths in the helix: n	3
Length of the flagella: L	nλ
Radius of flagella filament: r	100 nm

All parameters appear in mobility matrices as defined by Lauga *et al.* [44]

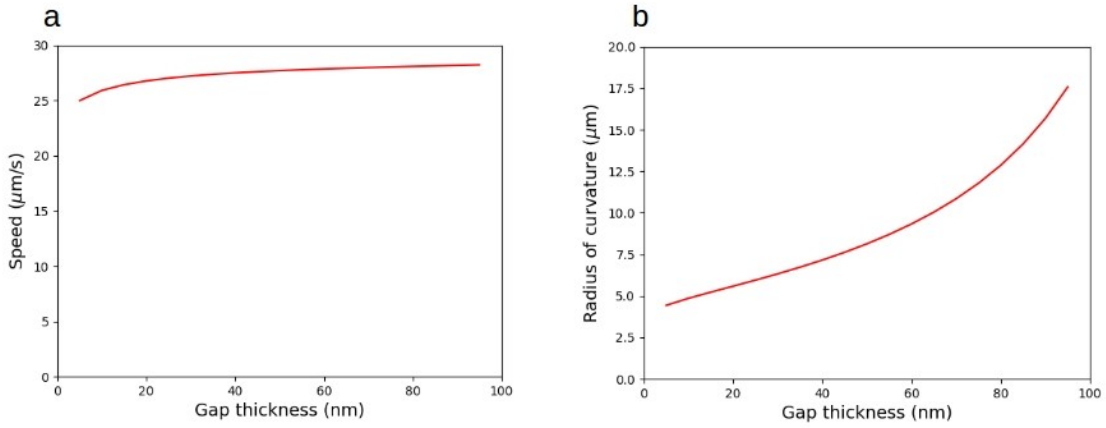

Figure A.2: Speed and radius of curvature as functions of the gap thickness, calculated from resistive force theory. (a) Speed vs gap thickness. The gap distance is from the bottom of the cell body to the solid surface below. Note a slight increase in speed with gap distance from 5nm to 40nm, but the swimming speed quickly approaches an upper limit. (b) Radius of curvature vs gap thickness. The radius of curvature increases sharply with gap thickness, as the hydrodynamic influence of the solid surface diminishes. The minimum distance from the surface is set to be 5 nm, below which distance the hydrodynamic model breaks down.

APPENDIX B

SUPPLEMENTARY INFORMATION FOR CHAPTER 4

B.1 Plotting the current vs voltage data (I-V curve)

I measured the electric current in the capillary channel originated with the application of the external DC voltage, as described in the Methods section chapter 4. The purpose of this measurement if at least twofold: 1. By repeating such measurements over multiple samples, the extent of variation informs us how sensitively the actual field strength in the middle of the capillary depends on the exact positions of the electrodes as they are connected to the capillary at both ends. 2. By monitoring the current over time, I learn about how stable the bacteria-containing liquid is, and what the proper time scale is for the experiments I performed. For 1, I realized that small changes in the electrodes inserted into the channel indeed leads to significant variation on the electric current. This amount of variation, by as much as $20 - 30\%$, sets the limit of accuracy for this experimental design. For 2, I noted a time dependence of the current in the sense that over ≈ 30 seconds under a fixed applied voltage, the resulting current tended to increase over time. This increase was probably due to some ionic effects that occur near the electrodes. The current would then stabilize for no more than two or three mins before it would drop down over longer time after air bubbles formed close to the electrodes.

As a consequence of this time dependence, I noted that when measuring current as a function of voltage in incremental steps, the results from previous measurements affect the subsequent measurements. To correct for this effect, I did three series of measurements of current with stepwise increases of voltage (+10 V per step) and then repeated the measurements 3 times with stepwise deceases, i.e. starting from the highest voltage (120 V) down to 0 V in decreasing steps (-10 V per step). The I-V curves for the two sequences of mea-

surements indeed show opposite curvatures, but averaging them yielded a proportional I-V curve, as it should be. Figure B.1 shows the plot of the I-V curve obtained by averaging all measurements ramping up and down in measurement steps over 3 cycles. The large error bars are notably due to different values between values acquired from the stepwise up as opposed to stepwise down measurements.

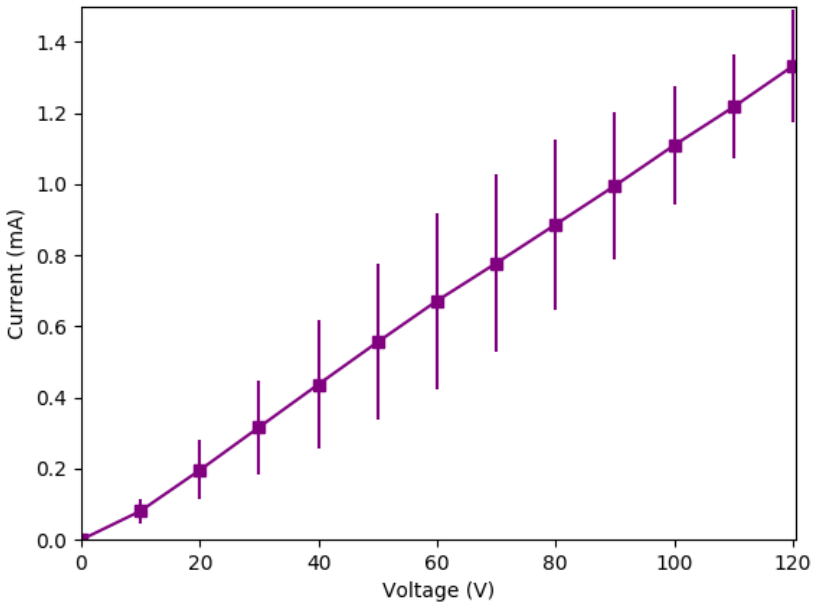

Figure B.1: I-V curve. Each data point was the average of six measurements: three with stepwise increase and three with stepwise decrease voltage steps. Error bars represent the standard deviation. The solid line is a trend connecting the dots.

B.2 Estimating the electrophoretic mobility of C. crescentus based on measurements of drift velocity

When driven by an electric field (E), the ratio between the velocity of motion (v) of a charged particle and the field is defined as the particles electrophoretic mobility (μ). In mathematical terms:

$$\mu = v/E \tag{B.1}$$

I measured the average drift velocity of six non-motile cells driven by the electric field of three applied voltages (80 V, 100V, 120 V) , with the results shown as a bar graph (Figure B.2). I estimated the electric field as the applied voltage divided by the length of the capillary channel (5 cm), ignoring the voltage drop in the proximity of the electrodes due to the effect commonly known as contact resistance. Thus, I was able to estimate the electrophoretic mobility (epm) of C. crescentus using Equation B.1. The results obtained are shown in Table B.1, which average to -1.4 μm.cm. V-1.s-1. This value is comparable to what is reported as -1.199 μm.cm. V-1.s-1 for E. coli grown in L-medium [87].

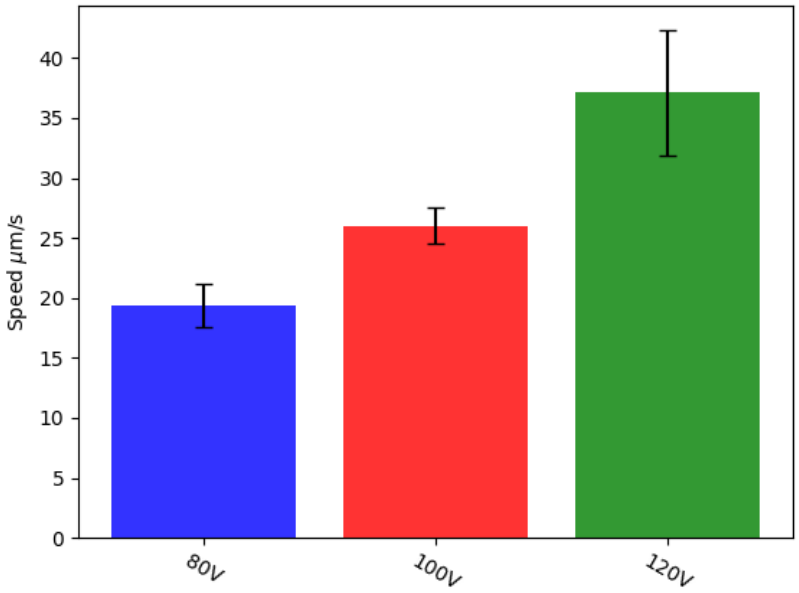

Figure B.2: Average drift velocity for non-swimming cells driven by the applied electric fields. The error bars represent standard deviations. The averages were taken for 6 cells at each voltage.

Table B.1: Estimated electrophoretic mobility at three applied voltages.

Voltage (V)	Electrophoretic mobility (μm.cm. V^{-1}.s^{-1})
80	-1.2
100	-1.4
120	-1.5

B.3 Estimating the electric force on bacteria

I estimate the electric force (F) driving the bacterial cells by applying the Stokes law for spherical particles moving in a viscous medium:

$$F = 6\pi r v \tag{B.2}$$

Here, η is the fluid viscosity, r is the radius of the spherical particle and v is the velocity of the driven motion. Taking 1 μm as a typical size scale for a bacterium radius, the dynamic viscosity of water (= 0.89 mPa.s) at room temperature and the average speed of 26 $\mu m/s$ for non-swimmers cells measured at 100 V (see Figure B.2), I obtain a driving force of about 0.4 pN (picoNewtons) at this voltage. This force is rather small. It can be provided by one or a few polymers transiently and perhaps non-specifically tethered on the solid surface. This crude estimate also explains why I noted only a small number of cells occasionally dislodged by the field applied in our experiments. With either more molecular tethers or stronger binding, the electric field applied might be insufficient to detach most attached cells. Such a weak force can also be applied by shear in typical microfluidic experiments.

APPENDIX C
BACTERIAL ROLLING MOTION AND CELLS STALLED TO A SOLID SURFACE

In addition to the dragging motion near a surface described in more detail in chapter 4. I also observed other interesting behaviors for bacterial motion, near to a solid boundary under the influence of an electric field. In particular, two of them are briefly described in this section: rolling motion and stalled cells.

C.1 Rolling motion

I noticed, along with undergraduate student Joy Zheng, cases of pre-divisional *Caulobacter crescentus* cells (i.e. cells prior to their division stage in which one cell reproduces giving birth to two cells) initially attached to the surface. A number of these cells had spinning motion and got detached under the application of the electric field (on the same order of magnitude as those described in chapter 4), but they kept spinning. Once such a cell gets detached, it will have a translation component in its trajectory, due to the electrokinetic effects. When coupled to the spinning motion it gives rise to a cell path that resembles a cycloid. We named this behavior as *rolling motion*. The presence of the spinning motion suggests that these cells remain close to the boundary, so that their flagella can roll around the surface, promoting the spinning.

Figure C.1 shows a timelapse sequence for a rolling motion pre-divisional cell. Figure C.2 illustrates what the trajectory of such a cell looks likes.

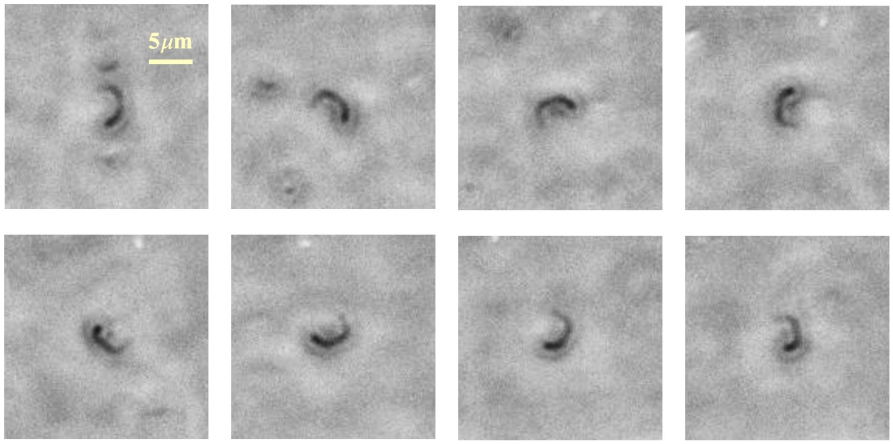

Figure C.1: Sequence of microscopic images of a pre-divisional *C. crescentus* cell performing rolling motion. One can follow the spinning motion by the geometrical orientation of the curved bacterial cell. Sequence should be read from left to right. Credit to image editing: Joy Zheng.

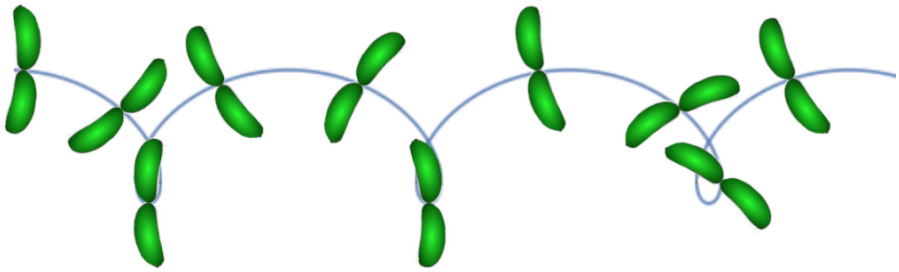

Figure C.2: Illustration of the cycloid trajectory for a rolling cell. These trajectories are a result of the coupling between the spinnig of the cell near the surface and the translational motion caused by the external electric field. Credit to image editing: Joy Zheng.

C.2 Stalled cells

An addition evidence for the alignment of bacterial cells (*C. crescentus* in the case of my experiments, to be more precise) under an electric field parallel to their boundary surface is noticed in the occurrence of cells initially spinning when there is no electric field applied, but that have their spinning suppressed under the application of the field, while orienting themselves along the field axis. Here the focus is on cells that do not get detached. The relevant fact in these cases is that when the field is turned off the spinning motion is re-

sumed. In other words, the electric field works as a switch to align the cells and prevent their spinning. Figure C.3 shows a timelapse sequence for a stalled cell.

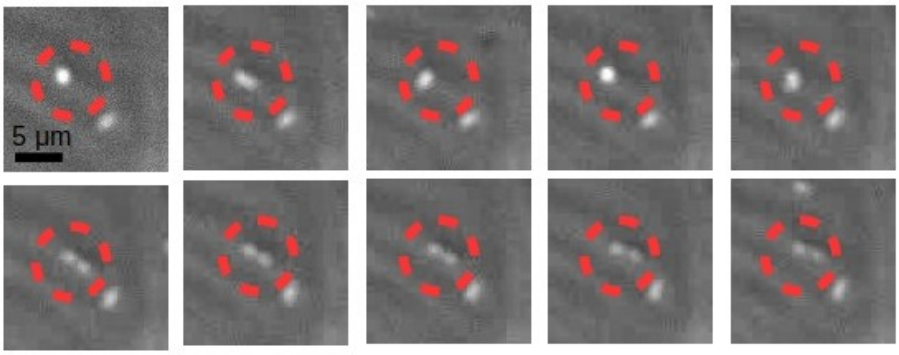

Figure C.3: Sequence of images of a cell initially spinning (no electric field applied) that gets oriented along the field once it is turned on, suppressing the spinning motion. Sequence should be read from left to right and consecutive pictures are 2 seconds apart in recording time. The initially spinning cell (inside the red dashed circle) reorients itself in the first five pictures, but remained nearly immobile in the last five pictures. There is an immobile cell outside the dashed circle. The field was applied for almost 30 seconds and once it was turned off the spinning motion was reestablished.

APPENDIX D
NUMERICAL SOLUTIONS TO POISSON-BOLTZMANN AND CONSERVED CHARGE POISSON-BOLTZMANN EQUATIONS

Studies the electrokinetic effects on a capillary channel filled with an ionic solution, with the system in equilibrium, are traditionally described in terms of the Poisson-Boltzmann (PB) equation. Wan et al [18] pointed out that in this approach there is no guarantee of conservation of charge within the computational domain. To solve this issue they reformulated the charge calculation and introduced the Conserved-Charge-Poisson-Boltzmann equation. Additionaly, in order to reproduce the electric double layer, characteristic in electrokinetic phenomena, they added a scalar *trap potential* active near the capillary walls. During the course of my phd studies, I dedicated some time to implement, from scratch, numerical solutions to these equations, given that the reference publication mentioned above numericaricaly works with the closed code software Comsol Multiphysics. In this section, I describe the general approach and reproduce graphical results.

D.1 Procedure to solve the Poisson-Boltzmann equation

As described in chapter 2, the ionic distribution on a given medium results in an elestrostatic potential, as described by the Poisson equation:

$$\nabla^2\psi = -\frac{e(p-n)}{\epsilon} \tag{D.1}$$

The Poisson-Boltzmann formulation takes place when the charge distributions are given by Boltzmann factors: $n = \alpha exp(e\phi/k_BT)$ and $p = \beta exp(-e\phi/k_BT)$. Where ϕ is the total electrostatic potential, coming from the ionic distribution, trap potential (see chapter 2) and eventual external potential.

Taking into account the Debye length ($\lambda_D = \sqrt{\frac{k_B T}{2 N_A e^2 I}}$) and a normalization of the total potential: $\bar{\phi} = e\phi/k_B T$:

$$\nabla^2 \bar{\phi} = \frac{1}{\lambda^2} sinh(\bar{\phi}) \tag{D.2}$$

For a simplified notation, from now on I will refer to $\bar{\phi}$ simply as ϕ.

In the following steps, it will be shown the Finite differences discretization of equation D.2 in cyllindrical coordinates (only dependant on the radial coordinate). The right hand side of D.2 will be replaced by: $F(\phi) = \frac{1}{\lambda^2} sinh(\bar{\phi})$.

$$\nabla^2 \phi = \frac{1}{r} \frac{\partial}{\partial r} (r \frac{\partial \phi}{\partial r}) = \frac{\partial^2 \phi}{\partial r^2} + \frac{1}{r} \frac{\partial \phi}{\partial r} \tag{D.3}$$

Hence, the discretization of D.2 can be written as follows, where the index *i* indicates the i-th elemenent on the Finite differences grid:

$$\frac{\phi_{i+1} - 2\phi_i + \phi_{i-1}}{(\Delta r)^2} + \frac{1}{r_i} \frac{\phi_{i+1} - \phi_{i-1}}{2(\Delta r)} = F(\phi_i) \tag{D.4}$$

The overall solution to D.4 requires solving for all points in the grid. Note that $r_i = i\Delta r$, where the discretization step Δr is given by: $\Delta r = a/lx$. Where *a* represents the radius of the channel and *lx* the number of grid points.

By looking at D.4, one element of concern is how to deal with the case when the radial coordinate is zero, since this equation has a r_i in one denominator. The general procedure which has been adopted in such situations is to apply $l'Hopital$ rule for $r = 0$.

$$\frac{1}{r} \frac{\partial \phi}{\partial r} \longrightarrow \frac{\partial^2 \phi}{\partial r^2} \tag{D.5}$$

Imposing the boundary condition $\frac{\partial \phi}{\partial r} = 0$, at $r = 0$ (Neumann Boundary condition), we have the discretization $\frac{\partial^2 \phi}{\partial r^2} = \frac{2(\phi_1 - \phi_0)}{(\Delta r)^2}$ at this point.

The numerical solution to the PB equation can be obtained by applying the Newton-

Raphson method, which consists of turning the equation to solve into a system of linear equations of the form: $A(\phi) = F(\phi)$, where here ϕ represents a vector matrix with all the values of the electrical potential along the grid. So, it is necessary to determine *A*, the matrix of coefficients.

In equation D.4, by taking $r_i = i\Delta r$ and multiplying both sides by $(\Delta r)^2$ we get:

$$(\phi_{i+1} - 2\phi_i + \phi_{i-1}) + \frac{\phi_{i+1} - \phi_{i-1}}{2i} = F(\phi_i)(\Delta r)^2 \tag{D.6}$$

When $r = 0$, considering the Neumann boundary condition, the equation is given by:

$$\frac{\partial^2\phi}{\partial r^2} = F(\phi_0) \longrightarrow \frac{2(\phi_1 - \phi_0)}{(\Delta r)^2} = F(\phi_0) \longrightarrow \phi_1 - \phi_0 = \frac{(\Delta r)^2 f(\phi_0)}{2} \tag{D.7}$$

I will call, from now on, the last right hand side of equation D.7 as $f(\phi_0)$. When $r = a$, the Dirichlet boundary condition $\phi_N = 0$ is imposed. Note that this value of ϕ_N enters in the calculation of the PB equation for $i = N - 1$.

From all the discussion above, we come to the conclusion that the matrix *A* is constructed as follows, $A[x][y]$ indicates the element A_{xy} of the matrix:

$A[i][i] = -2$

$A[i][i-1] = 1 - 1/(2i)$

$A[i][i+1] = 1 + 1/(2i)$

$A[0][0] = -1$

$A[0][1] = 1$

$A[lx-1][lx-2] = 1 - 1/[2(lx-1)]$

$A[lx-1][lx-1] = -2$

All other elements of *A* are zero. The iterative solution of the system is achieved from: $\phi_{n+1} = \phi_n - J^{-1}.F(\phi_n)$, where here *n* indicates the iteration step, *J* is the jacobian matrix: $J = A - \frac{\partial f(\phi_i)}{\partial \phi_j}$ and $F(\phi_n) = A\phi_n - f(\phi_n)$. Notice that here ϕ represents the vector matrix

with the values of the potential along the grid. Let $\Delta\phi_n = \phi_{n+1} - \phi_n$. Convergence is accomplished when $\Delta\phi_n < \epsilon$ (for some predefined criteria), at this point the iteration is stopped.

D.2 Procedure for numerical solution of the Conserved Charge Poisson-Boltzmann equation

The PB equation has inconsistencies with the PNP equations. In particular, for small (nano-sized) channels, PB cannot accomplished overall charge conservation within the computational domain. In order to deal with this issue Wan et al [18] proposed a new scheme to calculate the density of the charged particles:

$$n = n^o \frac{exp(e\phi/k_BT))}{\frac{1}{V}\int d\mathbf{x} exp(e\phi/k_BT)} \tag{D.8}$$

$$p = p^o \frac{exp(-e\phi/k_BT))}{\frac{1}{V}\int d\mathbf{x} exp(-e\phi/k_BT)} \tag{D.9}$$

Incorporating them into the format of the PB equation leads to the Conserved Charge Poisson-Boltzmann equation (CCPB) (equation D.10) in which, as the name suggests, charge conservation is accomplished.

$$\frac{1}{r}\frac{\partial}{\partial r}(r\frac{\partial\phi}{\partial r}) = \frac{ea^2n^o}{2\epsilon}[\frac{exp(e\phi/k_BT)}{\int_0^a r exp(e\phi/k_BT)dr} - \frac{exp(-e\phi/k_BT)}{\int_0^a r exp(-e\phi/k_BT)dr}] \tag{D.10}$$

A critical implication of the CCPB model is the fact that the occurrence of an electrical double layer does not come naturally. It requires some additional mechanism which causes separation of charge within the computational domain. The way Wan et al [18] circumvent this problem happens by introducing a surface potential trap (equations 2.3 and 2.4). This potential trap will be responsible for attracting or repelling ions to the region immediately

close to the channel solid-liquid interface, as given by the width of the trap.

To help simplifying the CCPB equation, an useful quantity is introduced in this framework, the chemical potential μ, definied as follows:

$$\mu = \frac{k_B T}{2e} ln[\frac{\int_0^a exp(e(\psi + f)/k_B T) r dr}{\int_0^a exp(-e(\psi + f)/k_B T) r dr}] \tag{D.11}$$

The chemical potential must be calculated in a self-consistent method along with the solution of the CCPB. To be precise, the CCPB equation is solved starting with an initial guess for μ, this gives the values of ψ, which are then used for a better estimation of μ. The cycle continues until convergence is reached.

Including the trap potential and the chemical potential, CCPB equation is written as:

$$\frac{1}{r}\frac{\partial}{\partial r}(r\frac{\partial \psi}{\partial r}) = \frac{en^\infty}{\epsilon}[exp(e(\psi - \mu + f)/k_B T) - exp(-e(\psi - \mu + f)] \tag{D.12}$$

The methodology to discretize equation D.12 is similar to what was done for PB, thus it will not be described here (n^∞ is the ionic concentration in the bulk of the capillary).

D.3 Graphs

In this section, I show some graphs produced from the numerical solutions of the PB and CCPB equations.

First, figure D.1 shows the dependence of the accuracy of PB with the radial size of the capillary. For larger channels (radius 2.4 μm) the results of both PB and CCPB coincide, whereas for much smaller channels (radius 10 nm) the discrepancy is evident.

The calculation can also vary other parameters, such as the solution pH or the salt concentration. Figure D.2 shows examples of these cases.

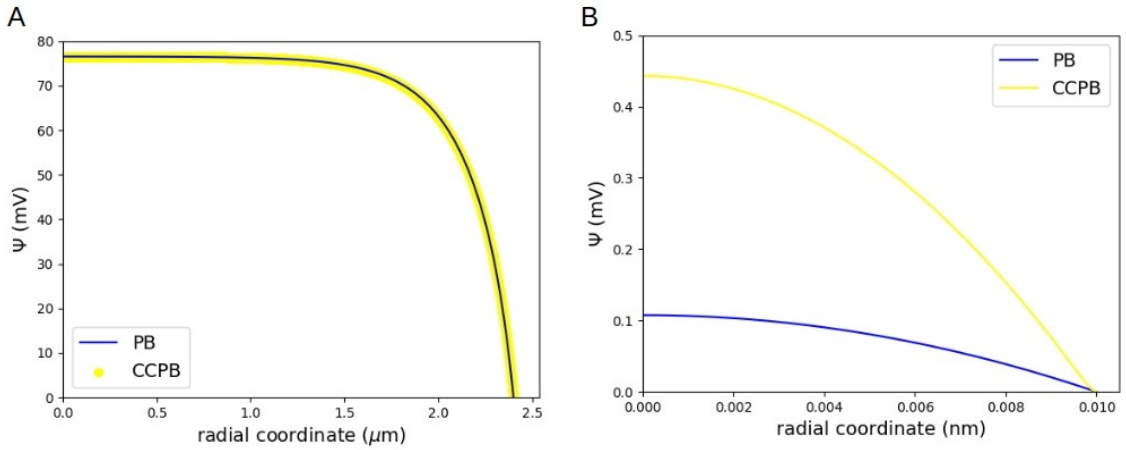

Figure D.1: Electrostatic potential due to ionic distribution as a function of the radial distance from the center of the capillary. A) radius of capillary: $2.4\mu m$. B) radius of capillary: 10 nm.

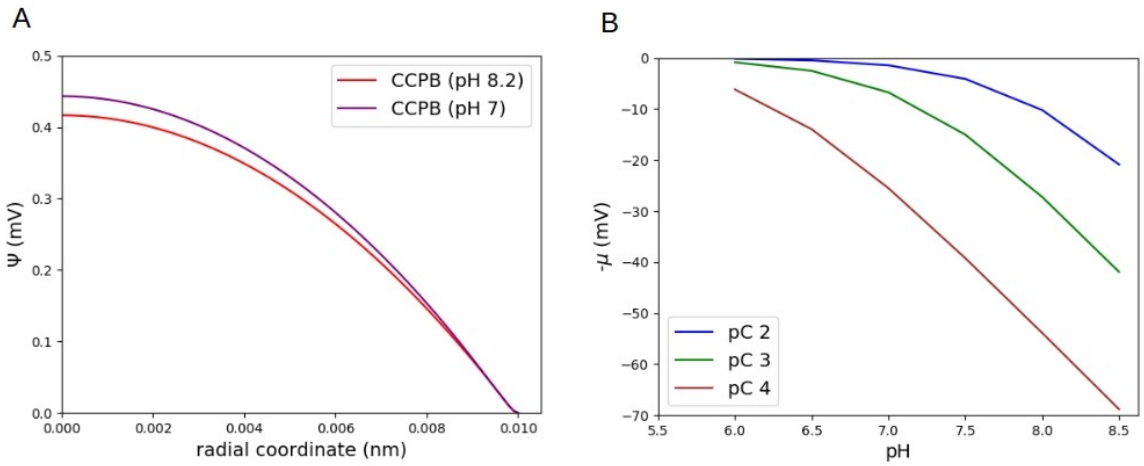

Figure D.2: CCPB calculations for a capillary with 10 nm radius. A) Plots of the ionic potential as a function of the radial coordinate for two values of pH. B) chemical potential (with negative sign) as a function of pH for three values of salt concentrations.)

REFERENCES

[1] E. M. Purcell, "Life at low reynolds number," *American Journal of Physics*, vol. 45, 1977.

[2] Q. Cai, Z. Li, Q. Ouyang, C. Luo, and V. D. Gordon, "Singly flagellated pseudomonas aeruginosa chemotaxes efficiently by unbiased motor regulation," *MBio*, vol. 7, e00013–1, 2016.

[3] S. C.X.L. W. L. Xie T. Altindal, *Proc. Natl. Acad. Sci.*, vol. 108, pp. 2246–2251, 2011.

[4] H. C. Berg, *Random walks in biology*, Expanded. Princeton University Press, 1993.

[5] E. Lauga, "Bacterial hydrodynamics," *Annu. Rev. Fluid Mech*, vol. 48, pp. 105–130, 2016.

[6] P. Nelson, *Biological physics*. W. H. Freeman and Company, 2004.

[7] J. A. Huber, D. A. Butterfield, and J. A. Baross, *FEMS Micro. Ecology*, vol. 43, pp. 393–409, 2003.

[8] C. A. Darling and P. A. Siple, *J. Bacteriol*, vol. 42, pp. 83–98, 1941.

[9] H. Z. et al, *Proc. Natl. Acad. Sci.*, vol. 113, 1500015005, 2016.

[10] D. B. Kearns, *Nat. Rev. Microbiol.*, vol. 8, 634644, 2010.

[11] A. Yang, W. S. Tang, T. Si, and J. X. Tang, "Influence of physical effects on the swarming motility of pseudomonas aeruginosa," *Biophysical journal*, vol. 112, no. 7, pp. 1462–1471, 2017.

[12] H. Darcy, "Les fontaines publiques de la vile de dijon," 1856.

[13] M. E. Rosti, S. Pramanik, L. Brandt, and D. Mitra, "The breakdown of darcys law in a soft porous material," *ArXiv*, 2019.

[14] C. W. MacMinn, E. R. Dufresne, and J. S. Wettlaufer, "Large deformations of a soft porous material," *Phys. Rev. Applied*, vol. 5, p. 044 020, 2016.

[15] D. L. Hu and J. W. M. Bush, "The hydrodynamics of water-walking arthropods," *J. Fluid Mech.*, vol. 644, pp. 5–33, 2010.

[16] J. W. Honschoten, N. Brunets, and N. R. Tas, "Capillary at the nanoscale," *Chem. Soc. Rev.*, vol. 39, 10961114, 2010.

[17] M. J. Desai and D. W. Armstrong, "Separation, identification, and characterization of microorganisms by capillary electrophoresis," *Microio. and Mol. Bio. Rev.*, vol. 67, pp. 38–51, 2003.

[18] L. Wan, S. Xu, M. Liao, C. Liu, and P. Sheng, "Self-consistent approach to global charge neutrality in electrokinetics: A surface potential trap model," *Phys. Rev. X*, vol. 4, p. 011 042, 2014.

[19] A. P. Berke, L. Turner, H. C. Berg, and E. Lauga, "Hydrodynamic attraction of swimming microorganisms by surfaces," *Phys. Rev. Letters*, vol. 101, p. 038 102, 2008.

[20] G. Li and J. X. Tang, "Accumulation of microswimmers near a surface mediated by collision and rotational brownian motion," *Phys. Rev. Letters*, vol. 103, p. 078 101, 2009.

[21] G. Li, J. Bensson, L. Nisimova, D. Munger, P. Mahautmr, J. X. Tang, M. R. Maxey, and Y. V. Brun, "Accumulation of swimming bacteria near a solid surface," *Phys.Rev.E*, vol. 84, p. 041 932, 2011.

[22] K. Drescher, J. Dunkel, L. H. Cisneros, S. Ganguly, and R. E. Goldstein, "Fluid dynamics and noise in bacterial cell-cell and cell-surface scattering," *Proc. Natl. Acad. Sci*, vol. 108, pp. 10 940–10 945, 2011.

[23] P. D. Frymier, R. M. Ford, H. C. Berg, and P. T. Cummings, "Three-dimensional tracking of motile bacteria near a solid planar surface," *Proc. Natl. Acad. Sci*, vol. 92, pp. 6195–6199, 1995.

[24] G. Li, L. K. Tam, and J. X. Tang, "Amplified effect of brownian motion in bacterial near-surface swimming," *Proc. Natl. Acad. Sci.*, vol. 105, pp. 18 355–18 359, 2008.

[25] M. A. Vigeant and R. M. Ford, "Interactions between motile escherichia coli and glass in media with various ionic strengths, as observed with a three-dimensional-tracking microscope," *Appl. Environ. Microbiol*, vol. 63, 34743479, 1997.

[26] W. R. DiLuzio, L. Turner, M. Mayer, P. Garstecki, D. B. Weibel, H. C. Berg, and G. M. Whitesides, "Escherichia coli swim on the right-hand side," *Nature*, vol. 435, 12711274, 2005.

[27] J. Mnnik, R. Driessen, P. Galajda, J. E. Keymer, and C. Dekker, "Bacterial growth and motility in sub-micron constrictions," *Proc. Natl. Acad. Sci*, vol. 106, pp. 14 861–14 866, 2009.

[28] S. A. Biondi, J. A. Quinn, and H. Goldfine, "Random motility of swimming bacteria in restricted geometries," *AICHE. J.*, vol. 44, pp. 1923–1929, 1998.

[29] M. Hennes, J. Tailleur, G. Charron, and A. Daerr, "Active depinning of bacterial droplets: The collective surfing of bacillus subtilis," *Proc. Natl. Acad. Sci*, vol. 114, pp. 5958–5963, 2017.

[30] A. Sokolov, L. D. Rubio, J. F. Brady, and I. S. Aranson, "Instability of expanding bacterial droplets," *Nature Comm.*, vol. 9, p. 1322, 2018.

[31] H. Wioland, J. D. F. G. Woodhouse, J. O. Kessler, and R. E. Goldstein, "Confinement stabilizes a bacterial suspension into a spiral vortex," *Phys. Rev. Lett.*, vol. 110, p. 268 102, 2013.

[32] I. Tuval, L. Cisneros, C. Dombrowski, C. W. Wolgemuth, J. O. Kessler, and R. E. Goldstein, "Bacterial swimming and oxygen transport near contact lines," *Proc. Natl. Acad. Sci*, vol. 102, 22772282, 2005.

[33] A. Sokolov and I. S. Aranson, "Rapid expulsion of microswimmers by a vortical flow," *Nature Comm.*, vol. 7, p. 11 114, 2016.

[34] L. Turner, R. Zhang, N. C. Darnton, and H. C. Berg, "Visualization of flagella during bacterial swarming," *Journal of Bact*, vol. 192, pp. 3259–3267, 2010.

[35] H. P. Zhang, A. Beer, E. L. Florin, and H. L. Swinney, "Collective motion and density fluctuations in bacterial colonies," *Proc. Natl. Acad. Sci.*, vol. 107, pp. 13 626–13 630, 2010.

[36] M. F. Copeland and D. B. Weibel, "Bacterial swarming: A model system for studying dynamic self-assembly," *Soft Matter*, vol. 5, pp. 1174–1187, 2009.

[37] W. M. D. Jr, "Bacterial adhesion: Seen any good biofilms lately?" *Clin. Microbio. Rev*, vol. 15, pp. 155–166, 2002.

[38] F. Jin, J. C. Conrad, M. S. Gibiansky, and G. C. L. Wong, "Bacteria use type-iv pili to slingshot on surfaces," *Proc. Natl. Acad. Sci*, vol. 108, pp. 12 617–12 622, 2011.

[39] G. A. OToole and R. Kolter, "Flagellar and twitching motility are necessary for pseudomonas aeruginosa biofilm development," *Mol. Microbiol.*, vol. 30, pp. 295–304, 1998.

[40] H.-C. Flemming, "Biofouling in water systems–cases, causes and countermeasures," *Applied microbiology and biotechnology*, vol. 59, no. 6, pp. 629–640, 2002.

[41] K. M. Ottemann and J. F. Miller, "Roles for motility in bacterial host interactions," *Mol. Microbiol.*, vol. 24, pp. 1109–1117, 1997.

[42] K. Cho, I. G. Hwang, Y. Kim, S. J. Lim, J. Lim, J. H. Kim, B. Gim, and B. M. Weon, "Low internal pressure in femtoliter water capillary bridges reduces evaporation rates," *Sci. Reports*, vol. 6, p. 22 232, 2016.

[43] R. W. Style, C. Hyland, R. Boltyanskiy, J. S. Wettlaufer, and E. R. Dufresne, "Surface tension and contact with soft elastic solids," *Nature Comm.*, vol. 4, p. 2728, 2013.

[44] E. Lauga, W. R. DiLuzio, G. M. Whitesides, and H. A. Stone, "Swimming in circles: Motion of bacteria near solid boundaries," *Biophys. J.*, vol. 90, 400412, 2006.

[45] K. M. Ford, J. D. Antani, A. Nagarajan, M. M. Johnson, and P. P. Lele, "Switching and torque generation in swarming e. coli," *Front. Microbiol.*, vol. 9, p. 2197, 2018.

[46] L. Lemelle, J. F. Palierne, E. Chatre, and C. Place, "Counterclockwise circular motion of bacteria swimming at the air-liquid interface," *Journal of Bact.*, vol. 192, 63076308, 2010.

[47] R. D. Leonardo, D. DellArciprete, L. Angelani, and V. Iebba, "Swimming with an image," *Phys. Rev. Lett.*, vol. 106, p. 038 101, 2011.

[48] M. Morse, A. Huang, G. Li, M. R. Maxey, and J. X. Tang, "Molecular adsorption steers bacterial swimming at the air/water interface," *Biophys. J*, vol. 105, pp. 21–28, 2013.

[49] R Cunningham, *Diffusion in gases and porous media*, First. Springer US, 1980.

[50] E. M. Johnson and W. M. Deen, "Hydraulic permeability of agarose gels," *AIChE Journal*, vol. 42, pp. 1220–1224, 1996.

[51] J. Wakita, S. Tsukamoto, K. Yamamoto, M. Katori, and Y. Yamada, "Phase diagram of collective motion of bacterial cells in a shallow circular pool," *Journal of the Phys. Soc. of Japan*, vol. 84, p. 124 001, 2015.

[52] D. R. Espeso, A. Carpio, and B. Einarsson, "Differential growth of wrinkled biofilms," *Phys. Rev. E*, vol. 91, p. 022 710, 2015.

[53] R. Long, M. S. Hall, M. Wu, and C. Y. Hui, "Effects of gel thickness on microscopic indentation measurements of gel modulus," *Biophys. J.*, vol. 101, pp. 643–650, 2011.

[54] E. A. Grice and J. A. Segre, "The skin microbiome," *Nat. Rev. Microbiol*, vol. 9, pp. 244–253, 2011.

[55] O. E. Petrova and K. Sauer, "Sticky situations: Key components that control bacterial surface attachment," *J. Bacteriology*, vol. 194, 24132425, 2012.

[56] H. Dang and C. R. Lovell, "Microbial surface colonization and biofilm development in marine environments," *J. Bacteriology*, vol. 80, pp. 91–138, 2016.

[57] C. Berne, C. K. Ellison, A. Ducret, and Y. V. Brun, "Bacterial adhesion at the single-cell level," *Nat. Rev. Microbiology*, vol. 16, pp. 616–627, 2018.

[58] K. Ottemann and J. F. Miller, "Roles for motility in bacterial-host interactions," *Mol Microbiol*, vol. 24, pp. 1109–1117, 1997.

[59] C. A. Rodesneya, B. Romana, N. Dhamania, B. J. Cooleya, P. Katirab, A. Touhamic, and V. D. Gordon, "Mechanosensing of shear by pseudomonas aeruginosa leads to increased levels of the cyclic-di-gmp signal initiating biofilm development," *PNAS*, vol. 114, 59065911, 2017.

[60] B. N. Anderson, A. M. Ding, L. M. Nilsson, K. Kusuma, V. Tchesnokova, V. Vogel, E. V. Sokurenko, and W. E. Thomas, "Weak rolling adhesion enhances bacterial surface colonization," *J. Bacteriology*, vol. 189, 17941802, 2007.

[61] J. Sjollema, H. C. van der Mei, C. L. Hall, B. W. Peterson, J. de Vries, L. Song, E. D. de Jong, H. J. Busscher, and J. J.T. M. Swartjes, "Detachment and successive re-attachment of multiple, reversibly-binding tethers result in irreversible bacterial adhesion to surfaces," *Sci. Reports*, vol. 7, p. 4369, 2017.

[62] E. P. Ipia, S. Otte, R. Pontier-Bres, D. Czerucka, and F. Peruani, "Bacteria display optimal transport near surfaces," *Nature Phys.*, vol. 15, pp. 610–615, 2019.

[63] A. G. Gristina, "Biomaterial-centered infection: Microbial adhesion versus tissue integration," *Science*, vol. 25, pp. 1588–1595, 1987.

[64] C. Gmes-Surez, H. J. Busscher, and H. C. V. der Mei, "Analysis of bacterial detachment from substratum surfaces by the passage of air-liquid interfaces," *App. and Env. Microbiol.*, vol. 67, 25312537, 2001.

[65] S. H. Hong, J. Jeong, S. Shim, H. Kang, S. Kwon, K. H. Ahn, and J. Yoon, "Effect of electric currents on bacterial detachment and inactivation," *Biotech. and Bioeng.*, vol. 100, pp. 379–386, 2008.

[66] I. Gall, M. Herzberg, and Y. Oren, "The effect of electric fields on bacterial attachment to conductive surfaces," *Soft Matter*, vol. 9, 24432452, 2013.

[67] A. T. Poortinga, J. Smit, H. C. van der Mei, and H. J. Busscher, "Electric field induced desorption of bacteria from a conditioning film covered substratum," *Biotech. and Bioeng.*, vol. 76, pp. 395–399, 2001.

[68] J. S. Poindexter, "The caulobacters: Ubiquitous unusual bacteria.," *MicroBiol. Rev.*, vol. 45, 123179, 1981.

[69] J. M. Skerker and M. T. Laub, "Cell-cycle progression and the generation of asymmetry in caulobacter crescentus," *Nat. Rev. Microbiology*, vol. 2, pp. 325–337, 2004.

[70] P. H. Tsang, G. Li, Y. V. Brun, L. B. Freund, and J. X. Tang, "Adhesion of single bacterial cells in the micronewton range," *PNAS*, vol. 103, 5764 5768, 2006.

[71] D. Bodenmiller, E. Toh, and Y. V. Brun, "Development of surface adhesion in caulobacter crescentus," *J. Bacteriology*, vol. 186, 4381447, 2004.

[72] G. Li and et al, "Surface contact stimulates the just-in-time deployment of bacterial adhesins," *Molecular Microbiology*, vol. 83, pp. 41–51, 2012.

[73] P. P. Lele, T. Roland, A. Shrivastava, Y. Chen, and H. C. Berg, "The flagellar motor of caulobacter crescentus generates when a more cell swims backward torque when a cell swims backwards," *Nature Phys.*, vol. 12, pp. 175–178, 2015.

[74] A. Persat, H. A. Stone, and Z. Gitai, "The curved shape of caulobacter crescentus enhances surface colonization in flow," *Nature Comm.*, vol. 5, p. 3824, 2014.

[75] J Newby, A. Schaefer, M. F. P Lee, and S. Lai, "Deep neural networks automate detection for tracking of submicron scale particles in 2d and 3d.," *PNAS*, vol. 115, pp. 9026–9031, 2018.

[76] M Morse, J Bell, G Li, and J. X. Tang, "Flagellar motor switching in caulobacter crescentus obeys first passage time statistics," *Phys. Rev. Letters*, vol. 115, p. 198 103, 2015.

[77] W. Shi, B. A. Stocker, and J. Adler, "Effect of the surface composition of motile escherichia coli and motile salmonella species on the direction of galvanotaxis," *J. Bacteriology.*, vol. 178, pp. 1113–1119, 1996.

[78] M. Gonin, E. M. Quardokus, D. O'Donnol, J. Maddock, and Y. V. Brun, "Regulation of stalk elongation by phosphate in caulobacter crescentus," *J. Bacteriology.*, vol. 182, pp. 337–347, 2000.

[79] S. Koyasu and Y. Shirakihara, "Caulobacter crescentus flagellar filament has a right-handed helical form," *J. Mol. Biol.*, vol. 173, pp. 125–130, 1984.

[80] B. Liu, M. Gulinoa, M. Morse, J. X. Tang, T. R. Powers, and K. S. Breuer, "Helical motion of the cell body enhances caulobacter crescentus motility," *PNAS*, vol. 111, 1125211256, 2014.

[81] S. Sharma and J. C. Conrad, "Attachment from flow of escherichia coli bacteria onto silanized glass substrates," *Langmuir*, vol. 30, 1114711155, 2014.

[82] S. Chattopadhyay, R. Moldovan, C. Yeung, and X. L. Wu, "Swimming efficiency of bacterium escherichia coli," *PNAS*, vol. 103, pp. 13 712–13 717, 2006.

[83] S. Hormeo and J. R. AriasGonzalez, "Exploring mechanochemical processes in the cell with optical tweezers," *Biology of the cell*, vol. 98, pp. 679–695, 2006.

[84] G. Li, C. Smith, Y. Brun, and J. X. Tang, "The elastic properties of the caulobacter crescentus adhesive holdfast are dependent on oligomers of n-acetylglucosamine," *J. Bacteriology*, vol. 187, pp. 257–265, 2005.

[85] G. Li and J. X. Tang, "Low flagellar motor torque and high swimming efficiency of caulobacter crescentus swarmer cells," *Biophys. Journal*, vol. 91, 27262734, 2006.

[86] M. Zaferani, S. H. Cheong, and A. Abbaspourrad, "Rheotaxis-based separation of sperm with progressive motility using a microfluidic corral system," *Proc. Natl. Acad. Sci.*, vol. 115, pp. 8272–8277, 2018.

[87] M. E. Bayer and J. L. S. Jr., "The electrophoretic mobility of gram-negative and gram-positive bacteria: An electrokinetic analysis," *Journal of General Microbiology*, vol. 136, pp. 867–874, 1990.